

1 **The full title: Developmental exposure to polychlorinated biphenyls prevents recovery**
2 **from noise-induced hearing loss and disrupts the functional organization of the inferior**
3 **colliculus.**

4
5 **The running title: PCBs prevent recovery from noise trauma**

6
7 Baher A. Ibrahim^{1,2}, Jeremy Louie¹, Yoshitaka Shinagawa^{1, 2}, Gang Xiao^{1,2,3}, Alexander R.
8 Asilador^{2,3}, Helen J. K. Sable⁶, Susan L. Schantz^{2,4} & Daniel A. Llano^{1,2,3,5*}

9 1- Department of Molecular & Integrative Physiology, the University of Illinois Urbana-Champaign,
10 Urbana, IL 61801, USA.

11 2- Beckman Institute for Advanced Science & Technology, the University of Illinois Urbana-
12 Champaign, Urbana, IL 61801, USA.

13 3- Neuroscience Program, the University of Illinois Urbana-Champaign, Urbana, IL 61801, USA.

14 4- Department of Comparative Biosciences, the University of Illinois Urbana-Champaign, Urbana,
15 IL 61801, USA.

16 5- Carle Illinois College of Medicine, the University of Illinois Urbana-Champaign, Urbana, IL
17 61801, USA.

18 6- The Department of Psychology, The University of Memphis, Memphis, TN 38152, USA.

19 * Correspondence: d-llano@illinois.edu

20 **Author contributions:**

21 Conceptualization, design supervision, funding acquisition, validation, investigation, B.A.I., S.L.S.,
22 D.A.L.; Data curation and visualization, B.A.I., D.A.L.; Formal analysis, B.A.I., Y.S., D.A.L.;

23 Methodology and validation, B.A.I., J.L., G.X., A.R.A., H.J.K.S., S.L.S., D.A.L.; Writing - original
24 draft, B.A.I.; Writing - review and editing, B.A.I., D.A.L.; Project administration, D.A.L.

25

26 **Abstract:**

27 Exposure to combinations of environmental toxins is growing in prevalence, and therefore
28 understanding their interactions is of increasing societal importance. Here, we examined the
29 mechanisms by which two environmental toxins – polychlorinated biphenyls (PCBs) and high-
30 amplitude acoustic noise – interact to produce dysfunction in central auditory processing. PCBs
31 are well-established to impose negative developmental impacts on hearing. However, it is not
32 known if developmental exposure to this ototoxin alters the sensitivity to other ototoxic exposures
33 later in life. Here, male mice were exposed to PCBs in utero, and later as adults were exposed to
34 45 minutes of high-intensity noise. We then examined the impacts of the two exposures on
35 hearing and the organization of the auditory midbrain using two-photon imaging and analysis of
36 the expression of mediators of oxidative stress. We observed that developmental exposure to
37 PCBs blocked hearing recovery from acoustic trauma. In vivo two-photon imaging of the inferior
38 colliculus revealed that this lack of recovery was associated with disruption of the tonotopic
39 organization and reduction of inhibition in the auditory midbrain. In addition, expression analysis
40 in the inferior colliculus revealed that reduced GABAergic inhibition was more prominent in
41 animals with a lower capacity to mitigate oxidative stress. These data suggest that combined
42 PCBs and noise exposure act nonlinearly to damage hearing and that this damage is associated
43 with synaptic reorganization, and reduced capacity to limit oxidative stress. In addition, this work
44 provides a new paradigm by which to understand nonlinear interactions between combinations of
45 environmental toxins.

46

47

48

49 **Significance statement:**

50 Exposure to common environmental toxins is a large and growing problem in the population. This
51 work provides a new mechanistic understanding of how the pre-and postnatal developmental
52 changes induced by polychlorinated biphenyls could negatively impact the resilience of the brain
53 to noise-induced hearing loss later in adulthood. The use of state-of-the-art tools, including in vivo
54 multiphoton microscopy of the midbrain helped in identifying the long-term central changes in the
55 auditory system after the peripheral hearing damage induced by such environmental toxins. In
56 addition, the novel combination of methods employed in this study will lead to additional advances
57 in our understanding of mechanisms of central hearing loss in other contexts.

58

59

60

61

62

63

64

65

66

67

68

69

70

71

72

73

74

75 **Introduction:**

76 Overexposure to occupational noise is considered one of the main factors negatively impacting
77 hearing in the USA and Europe and is growing in prevalence (Bergström and Nyström, 1986;
78 Daniell et al., 2006; Ding et al., 2019). Contamination of the environment with ototoxic chemicals
79 could also exacerbate the effect of noise-induced hearing loss (NIHL). Polychlorinated biphenyls
80 (PCBs) are associated with hearing loss and other health deficits (Powers et al., 2006; Powers et
81 al., 2009; Min et al., 2014) (Wu et al., 1984; Safe, 1993; Goldey et al., 1995; Morse et al., 1996;
82 Brouwer et al., 1999; Xie et al., 2019). PCBs were banned by the U.S. Environment Protection
83 Agency (Ross, 2004) but are highly chemically stable, which has led to widespread and persistent
84 environmental contamination (Beyer and Biziuk, 2009). Given that PCBs can enter the placenta
85 and breast milk (Jacobson et al., 1984), they also pose a developmental threat (Guo et al., 2004)
86 including to the cochlea (Uziel, 1986; Goldey et al., 1995; Wong et al., 1997; Knipper et al., 2000;
87 Song et al., 2008) and developmental exposure to PCBs impairs the hearing of humans and
88 animals (Goldey et al., 1995; Herr et al., 1996; Crofton and Rice, 1999; Crofton et al., 2000; Lasky
89 et al., 2002; Powers et al., 2006; Kenet et al., 2007; Powers et al., 2009; Jusko et al., 2014; Min
90 et al., 2014; Palkovičová Murínová et al., 2016; Sadowski et al., 2016; Lee et al., 2021). Given
91 the high population prevalence of dual exposure to PCBs and noise, the objective of the current
92 study was to examine the interaction between developmental exposure to PCBs and NIHL later
93 in adulthood in both the peripheral and central auditory systems. We, therefore, exposed mice to
94 PCBs and noise overexposure similar to the sequence that also occurs in humans: prenatal +
95 breastmilk exposure to PCBs followed by adult overexposure to noise. Given previous work
96 showing changes in inhibitory tone in the major auditory integration center in the midbrain, the
97 inferior colliculus (IC), after either PCB or noise overexposure (Abbott et al., 1999; Dong et al.,
98 2010b; Dong et al., 2010a; Auerbach et al., 2014; Poon et al., 2015; Bandara et al., 2016;
99 Sadowski et al., 2016; Knipper et al., 2021; Lee et al., 2021), we examined inhibitory neuronal
100 activity in the IC of adult mice exposed to PCBs perinatally, noise in adulthood, or both, using

101 two-photon imaging of the IC *in vivo*. In addition, given previous work showing that pathological
102 disruptions of inhibition may be related to oxidative stress (as reviewed (Ibrahim and Llano,
103 2019)), we measured markers of oxidative stress in the IC. We observed that the developmental
104 exposure to PCBs impaired the hearing of the male mice to low frequency pure tones. While
105 developmental exposure to PCBs did not exacerbate the NIHL, it blocked the hearing recovery
106 one week from acoustic trauma at the same low frequencies. Using two-photon imaging,
107 developmental exposure to PCBs and high level of noise later in adulthood showed a disruption
108 of the tonotopic maps of the dorsal cortex of the IC (DCIC), which was characterized with a wide
109 non-responsive zone to acoustic stimulation, increase in the stimulus level required to evoke the
110 cellular activity of the responsive cells, and the downregulation of inhibition, which was associated
111 with low resilience to oxidative stress. These results suggest nonlinear interactions between the
112 developmental exposure to PCBs and NIHL at the level of both peripheral and central auditory
113 system.

114 **Materials and methods:**

115 **Animals:**

116 Wild-type female Swiss Webster (SW) mice (Jackson lab, # 000689), approximately three months
117 of age, were used for the initial PCBs dosing. The female mice were bred with male GAD67-GFP
118 knock-in mice of the same SW background (developed and shared with permission from Dr.
119 Yuchio Yanagawa at Gunma University and obtained from Dr. Douglas Oliver at the University of
120 Connecticut) to produce offspring where GFP is exclusively expressed in the GABAergic cells
121 (Tamamaki et al., 2003) to visualize and distinguish the GABAergic cells from non-GABAergic
122 cells in the offspring. All procedures were performed following protocol #19104, which was
123 approved by the Institutional Animal Care and Use Committee (IACUC) at The University of Illinois
124 at Urbana-Champaign. The mice were individually housed in standard plastic cages with corncob

125 bedding, in a temperature- and a humidity-controlled room that was maintained on a 12-h
126 light/dark cycle (lights off at 1900 h). Food and tap water were available ad libitum.

127 **PCB exposure:**

128 The timeline of the experimental procedures is shown in figure 1A. Given that eating PCB-
129 contaminated fish was reported to be one of the main routes of human exposure to PCBs
130 (Fitzgerald et al., 1996; Fitzgerald et al., 1998), the Fox River PCB mixture, which mimics the PCB
131 levels in contaminated Walleye fish from the Fox River of Northeast Wisconsin, was used in this
132 study as previously done on rats (Powers et al., 2006; Sadowski et al., 2016; Lee et al., 2021).
133 This PCB mixture consisted of 35% Aroclor 1242, 35% Aroclor 1248, 15% Aroclor 1254, and 15%
134 Aroclor 1260 (Kostyniak et al., 2005). In study phase one, the developmental toxicity of PCBs on
135 hearing was examined in mice. The female mice were randomly assigned to three different groups
136 receiving daily PCBs doses of 0, 6, or 12 mg/kg body weight. A dose of 6 mg/kg PCBs was
137 reported to impair hearing in rats compared to lower doses (Powers et al., 2006). Exposure began
138 28 days before mating and continued until pups were weaned on postnatal day 21 (P21). The
139 PCBs mixture was diluted in corn oil (Mazola®) and pipetted onto 40-50 mg of vanilla wafer cookie
140 (Nilla Vanilla Wafers®) at a volume of 0.4 ml/kg. At the dosing time, each female mouse was
141 taken to a separate empty plastic cage (with no bedding to easily identify the cookie pellet) at
142 approximately 1400 h. The PCBs-contaminated cookie was placed in the center of its dosing cage
143 allowing the animal to fully eat it. Aligned with the previous report, it was found that the average
144 time for the mouse to fully eat the cookie was 30 minutes (Cadot et al., 2012). The same dosing
145 paradigm was followed in study phase II, which examined the interaction between developmental
146 exposure to PCBs and noise exposure in adulthood.

147 **Breeding:**

148 In all study phases, each female mouse was paired with an unexposed GAD67-GFP male mouse
149 of a SW background. After breeding, the females were monitored once daily for the presence of
150 a sperm plug (i.e., gestational day 0), and mice were paired for 15 consecutive days regardless

151 of whether a sperm plug was observed. The pups at day 7 of age were phenotyped for the
152 presence of GFP under a fluorescence microscope via transcranial imaging (Tamamaki et al.,
153 2003). This process was done by gently handling and placing each pup under a fluorescence
154 microscope. GFP-positive pups were detected by examining the green fluorescent signals of the
155 GFP (excitation: 472/30 nm, dichroic 505 nm, emission 520/35 nm long pass). Then, only GFP-
156 positive pups were kept. After weaning, one male and one female from each litter were randomly
157 selected to serve as subjects for this study. The pups were housed in same-exposure and same-
158 sex cages of up to 5 mice/cage.

159 **Noise exposure:**

160 In study phase two, the paradigm of noise exposure was selected to induce a TTS (Amanipour et
161 al., 2018). Whether the animals were developmentally exposed to PCBs or not, the three-month-
162 old animals were all exposed to 110 dB SPL broadband noise for 45 minutes (Fig. 2A. The noise
163 was delivered by Fostex super tweeter (T925A, Fostex Corp, Japan) using a pre-amplifier (SLA1,
164 Studio linear amplifier). The noise exposure was done under anesthesia induced with a mixture
165 of ketamine hydrochloride (100 mg/kg), xylazine (3 mg/kg), and acepromazine (3 mg/kg) to avoid
166 the possible occurrence of audiogenic seizures as shown before in rats (Poon et al., 2015;
167 Bandara et al., 2016). The exposure was done in a sound-attenuated dark room and was
168 supervised from outside using an IR camera (ELP HD digital camera). The anesthesia was
169 maintained during noise exposure using only ketamine (100 mg/kg).

170 **ABR:**

171 As previously described (Lee et al., 2021), the ABR of three-month-old offspring was examined
172 with or without noise exposure. In study phase one, the ABR was taken from the offspring at three
173 months of age. In study phase two, the ABR was taken before (Pre-NIHL), immediately after
174 (Post-NIHL-day 0), one week after (Post-NIHL-day 7), and four months after (Post-NIHL-day 120)
175 noise exposure. ABRs were obtained at frequencies of 4, 5, 8, 10, 14, 16, 20, and 24 kHz as well
176 as white noise. Animals were anesthetized with the same (ketamine hydrochloride, xylazine, and

177 acepromazine) mixture, and the anesthesia was maintained during ABR measurements using
178 only ketamine (100 mg/kg). Three subdermal electrodes were inserted [(one at the vertex (active
179 electrode), one behind the right ear (reference electrode), and one behind the left ear (the ground
180 electrode)]. The mouse was placed 5 cm from the speaker on a heating pad. Stimuli were
181 presented using a Tucker-Davis (TDT) system 3 (Alachua, FL, USA), ES1 free-field speaker, with
182 waveforms being generated by RPvdsEx software. The output of the TDT speaker was calibrated
183 at all the relevant frequencies, using a PCB 377A06 microphone (Depew, NY, USA) and a
184 Svantek 977 Sound & Vibration Analyser (Warsaw, Poland). Each frequency was presented for
185 5 ms (3 ms flat with 1 ms for both rise and fall times), at a rate of 21 Hz with a 45 ms analysis
186 window. The ABR waveform was collected with TDT RA4PA Medusa Preamps with a 3 Hz -5 kHz
187 filter and was averaged over 500 repeats for one sound stimulus. The visual inspection of the
188 deflections of ABR within 10 ms from the stimulus's onset continued until I-V waves were no
189 longer present in the waveform. Although 86 dB SPL was the loudest level used, some animals
190 were deaf at this level indicated by no identified ABR signals. To assign a numerical value for
191 these deaf animals at 86 dB SPL sounds, a 90 dB SPL value was assumed as a threshold for
192 those animals across different exposures. The reading of the ABR thresholds was conducted by
193 an independent experimenter who was blind to the corresponding exposure groups of the
194 animals. After ABR measurement, each animal was kept on a heating pad until a full recovery,
195 then the animal was moved back to its home cage. After noise exposure, the hearing threshold
196 shift was calculated on days 0, 7, and 120 indicated by $[(\text{Post-NIHL-day } x) - (\text{Pre-NIHL})]$, where
197 x is the day after noise exposure i.e (0, 7, or 120).

198 **Viral injection:**

199 In study phase two, all mice across all groups were injected with AAV1.Syn.NES-
200 jRGECO1a.WPRE.SV40 (100854-AAV1, Addgene) into the IC after the last ABR session (Post-
201 NIHL-day 7). The virus drives the expression of the jRGECO1a in non-GABAergic and GABAergic
202 cells via synapsin (*Syn*) promoter. The detailed surgical procedures were described before

203 (Vaithiyalingam Chandra Sekaran et al., 2021). In brief, the surgery was done under aseptic
204 techniques. Mice were firstly anesthetized intraperitoneally with the (ketamine hydrochloride,
205 xylazine, and acepromazine) mixture. The anesthesia was maintained during the surgery using
206 only ketamine (100 mg/kg). Then the mouse was placed into a Kopf Model 940 Small Animal
207 Stereotaxic Instrument with a digital readout. After shaving and disinfecting the head with
208 Povidone–iodide and 70% ethanol, a longitudinal incision was made in the scalp. The underneath
209 surrounding tissue was injected with lidocaine (2% Covetrus, United States) intradermally as a
210 local anesthetic. Also, the mice were injected with carprofen (3 mg/kg, Henry Schein Melville, NY,
211 United States) subcutaneously as an analgesic for postoperative pain management. To protect
212 the eyes from drying an ophthalmic ointment was applied. A small craniotomy was made over the
213 IC targeting the DCIC using a surgical drill following these coordinates from lambda ($x = 0.65 -$
214 0.9 mm, $y = 0.9$ mm, and $z = 0.4$ mm). Glass micropipettes (3.5-inches, World Precision
215 Instruments, Sarasota, FL) were pulled using a micropipette puller (P-97, Sutter Instruments,
216 Novato, CA) and broken back to a tip diameter between 35 and 50 μm . The micropipette was
217 filled with mineral oil (Thermo Fisher Scientific Inc, Waltham, MA) and attached to a pressure
218 injector (Nanoliter 2010, World Precision Instruments, Sarasota, FL) connected to a pump
219 controller (Micro4 Controller, World Precision Instruments, Sarasota, FL). The amount of the virus
220 solution was then withdrawn by a pressure injector, and 450 nL of the viral solution with titer equal
221 to 1.7×10^{13} vgc/ μL was injected into the DCIC at a flow rate (50 nl/minute). After the injection, the
222 micropipette was kept in its place for another 5 minutes to avoid any solution retraction. The
223 incision was then sutured using 5/0 thread-size, nylon sutures (CP Medical, Norcross, GA). After
224 the surgery, the animals were kept on a heating pad for recovery. After awakening, animals were
225 returned to their home cages.

226 **Craniotomy surgery for placing the cranial window and head post:**

227 The craniotomy was done four months after the viral injection, and the general procedures of
228 craniotomy were previously described (Goldey et al., 2014), with modifications to place

229 craniotomy over the IC. Before surgery, mice were anesthetized with the (ketamine hydrochloride,
230 xylazine, and acepromazine) mixture. The anesthesia was maintained during the surgery and
231 imaging using only ketamine (100 mg/kg). To prevent neural edema during or after the
232 craniotomy, an intramuscular injection of dexamethasone sodium (4.8 mg/kg) was given just
233 before the surgery using an insulin syringe. After placing the animal in the stereotaxic apparatus
234 (David Kopf Instruments, USA), both eyes were protected by applying Opti care lubricant eye gel
235 (Aventix Animal Health, Canada). The hair on the scalp was then removed by massaging the
236 scalp with a depilatory cream (Nair) using a cotton-tipped applicator and leaving the cream on the
237 scalp for 4-5 minutes. The cream was then removed by a thin plastic sheet (flexible ruler) to leave
238 a hair-free area on the scalp. The remaining tiny hairs were then removed by alcohol swab and
239 the area was then sterilized by applying 10% Povidone Iodine (Dynarex, USA) using a sterile
240 cotton-tipped applicator. The medial incision was made with a scalpel blade #10, and 0.2 ml of
241 0.5% lidocaine was injected intradermally into the scalp. The skin extending from the medial line
242 to the temporalis muscle was completely removed using a pair of micro scissors to produce a
243 wide skinless area above the skull. A pair of no. 5/45 forceps were used to remove any remaining
244 periosteum. The remaining dried or firmly attached pieces of periosteum were removed with a
245 scalpel blade #10. The skull was cleaned with sterile saline and dried with gently pressurized air.
246 Using the stereotaxic apparatus, a wide area of ~3 x 4 mm above the left IC was made. A micro
247 drill bit (Size #80, Grainger, USA) was used to drill through the skull starting from the rostral-lateral
248 region to lambda. To prevent overheating of the superficial brain tissues and to mitigate the
249 occasional spurts of skull bleeding during the drilling, ice-cold sterile saline was used to
250 intermittently irrigate the surface. A stream of pressurized air was also applied during the drilling
251 procedure to prevent overheating and remove the debris produced by the drilling. Caution was
252 taken not to pierce the dura when performing the craniotomy while crossing the sagittal or the
253 lambdoid sutures to avoid damaging the underlying sinuses. After drilling, the skull was irrigated
254 in sterile saline and the bone flap (the undrilled bone over the craniotomy area) was gently

255 examined for complete separation from the rest of the skull. Using a pair of no. 5/45 forceps, the
256 bone flap was gently removed. To control the bleeding if it occurred, a piece of sterile hemostatic
257 gel (Adsorbable Gelatin Sponge USP, Haemosponge, GBI, India) which was pre-soaked in ice-
258 cold saline, was applied to the bleeding spot. Once the bleeding ceased, the brain was kept
259 covered in sterile saline. In some surgeries, the dura was peeled off from the surface of the IC
260 while removing the bone flap. In the surgeries where the dura remained intact, a Bonn microprobe
261 (F.S.T, Germany, Item # 10032-13) was used to pierce the dura in an area that is not above the
262 IC and devoid of cortical vasculature (e.g., a part of exposed cerebellum). After piercing, the dura
263 was carefully and gently lifted, and a pair of no. 5/45 forceps were used to grab the dura to gently
264 tear it to the extent of the transverse sinus to avoid bleeding. The cover glass was secured by a
265 wooden trimmed piece of sterile cotton swab by gently pressing the cover glass from the top. A
266 titanium head post as described before (Goldey et al., 2014) was glued carefully on the top of the
267 skull to be at the same level as the cover glass following the manufacturer's instructions, the C&B
268 Metabond (Parkell, Japan).

269 **Two-photon imaging.**

270 Immediately after surgery, the anesthetized animal was taken and secured under the microscope
271 objective by clamping the arms of the head post to two perpendicular metal posts mounted on the
272 microscope stage. A custom-built 2P microscope was used. The optical and the controlling
273 components were supplied from Bruker, Olympus, and Thorlabs. The imaging of the DC was
274 made using a 20x water-immersion objective (LUMPlanFI/IR, 20X, NA: 0.95, WD: 2 mm; Olympus
275 Corporation, Tokyo, Japan). Since the jRGECO1a calcium indicator was expressed in non-
276 GABAergic and GABAergic neurons, and the GFP was only expressed in the GABAergic cells in
277 the GAD67-GFP knock-in mouse, this was a good tool to distinguish the GABAergic (Green and
278 red signals) from non-GABAergic cells (Red signals only). For imaging both the GFP or
279 jRGECO1a signals, the excitation light was generated by InSight X3 laser (Spectra-Physics

280 Lasers, Mountain View, CA, USA) tuned to a wavelength of 920 or 1040 nm, respectively. A layer
281 of a 1:1 mixture of Multipurpose wavelengths ultrasound gel (National therapy, Canada) with
282 double deionized water was used to immerse the objective. This gel was able to trap the water
283 and reduce its evaporation during imaging. The emitted signals were detected by a photomultiplier
284 tube (Hamamatsu H7422PA-4, Japan) following a t565lp dichroic and a Chroma barrier
285 et525/70m filter for GFP and et595/50m filter for jRGECO1a signals. Images (512x512 pixels)
286 were collected at a frame rate of 29.9 Hz at the resonant galvo mode. Data were collected from
287 the dorsal surface of the IC by scanning the surface of the IC based on the GFP and jRGECO1a
288 signals through the medial and lateral horizons of the IC. Generally, each field of view was
289 selected based on the expression of jRGECO1a and being acoustically active using a search
290 stimulus that was 500 ms broadband noise with zero modulation at 80 dB SPL. The frame timing
291 of the scanner and the sound stimuli were both digitized and time-locked using a Digidata 1440A
292 (Molecular Devices, Sunnyvale, CA, USA) with Clampex v. 10.3 (Molecular Devices, Sunnyvale,
293 CA, USA).

294 **Acoustic stimulation:**

295 Using a custom-made MATLAB (The MathWorks, Natick, MA, USA) code, 500 ms pure tones
296 were generated. Each pure tone is one of the thirty-five (5x7) combinations of sound pressure
297 levels (80, 70, 60, 50,40 dB SPL) and carrier frequencies (5000-40000 Hz with a half-octave gap)
298 that was presented with a cosine window. Each run is composed of these 35 combinations that
299 were played in random sequence to the mice with a 600 ms interstimulus interval by a TDT RP2.1
300 processor (Tucker-Davis Technologies, US) and delivered by a TDT ES1 speaker (Tucker-Davis
301 Technologies, US). Thus, stimuli were delivered every 1100 ms. Given the relatively fast kinetics
302 of rGECO1a compared to earlier indicators (half decay time ~300 ms (Dana et al., 2016), this
303 interstimulus interval allowed for relatively dense sampling of stimulus space with minimal

304 carryover of calcium waveforms between stimuli. Each animal was presented with different runs
305 (mostly 9 runs on average). Each run has a different random sequence of the 35 combinations.

306 The output of the TDT ES1 speaker was calibrated using a PCB 377A06 microphone (Depew,
307 NY, USA), which feeds SigCal tool to generate a calibration file for all tested frequencies (5-40
308 kHz). To enable the custom-made MATLAB code to read this calibration file, the values were first
309 processed by MATLAB signal processing toolbox (sptool) to generate a 256-tap FIR filter to apply
310 the calibration using the following parameters [arbitrary magnitudes, least square, order: 256,
311 sampling rate: 97656.25, frequency vector (5-40 kHz), amplitude vector (40-80 dB SPL), and
312 weight vector [ones (1,128)].

313 **Data processing:**

314 *Data collection:* The data were collected as separate movies (512x512 pixels) in a resonant galvo
315 mode. Depending on the amplitude and frequency combinations for each type of acoustic
316 stimulus, 40 seconds was assigned as a movie's length for pure tone (35 stimulus combinations).
317 Using ImageJ software (<https://imagej.nih.gov/ij/>), the z-projection was used to compute one
318 single image representing either the sum, the standard deviation, or the median of all the image
319 sequences in the movie. Based on these single images, the region of interest (ROI) was manually
320 drawn around each detectable cell body.

321 *Motion Correction and Filtering:* The imread function from the OpenCV library was used in
322 grayscale mode to import images into a numpy array from a single folder containing TIFF images.
323 The array was then exported as a single TIFF stack into a temporary folder using the mimwrite
324 function from the imageio library, and the process was repeated for each folder. The NoRMCorre
325 algorithm (Pnevmatikakis and Giovannucci, 2017) embedded in the CalmAn library (Giovannucci
326 et al., 2019) was used to apply motion correction to each of the TIFF files. The data were then
327 imported into a numpy array, rounded, and converted to 16-bit integers. The images were filtered

328 using a 2D Gaussian filter with a sigma value of 1 (Surface View) / 2 (Prism View) in each
329 direction, then a 1D Gaussian temporal filter with a sigma value of 2 was applied using the
330 `ndimage.gaussian_filter` and `ndimage.gaussian_filter1d` function from the `scipy` library,
331 respectively.

332 *Data Extraction:* The ROI sets, which were manually created using ImageJ, were imported using
333 the `read_roi_zip` function from the `read_roi` library. The sets were then used to create two masks;
334 one mask was used as a replica of the ROIs and the second mask was made around the original
335 ROI (roughly four times larger in the area). The smaller mask was applied to find the average
336 pixel value within each ROI, while the larger mask was applied to find the average pixel value of
337 the neuropil. The neuropil correction was applied using the following equation (Akerboom et al.,
338 2012);

339
$$\text{Corrected value} = \text{Date value} - (0.4 \times \text{Neuropil value})$$

340 $\Delta f/f$ values were then calculated by using the following equation.

341
$$\frac{\Delta f}{f} = \frac{(\text{Peak value} - \text{Background value})}{\text{Background value}}$$

342 where the background value is the slope estimating the background levels with fluorescence
343 bleaching factored in. The data were then reorganized so that all segments with the same stimulus
344 frequency and stimulus amplitude were grouped.

345 *Cell Flagging:* The correlation coefficient between each of the trials was calculated using the `stats.`
346 `Pearsonr` function from the `scipy` library. The average correlation coefficient was calculated for
347 each stimulus frequency and stimulus amplitude. Similar to previous work (Wong and Borst,
348 2019), if the average correlation coefficient was above the threshold of 0.6, the cell was flagged
349 as being responsive to that stimulus combination of frequency and amplitude, and the best

350 frequency, which was defined as pure tone frequency that evoked the highest average response
351 across all sound levels, was calculated for the cell (Barnstedt et al., 2015).

352 *Tonotopic Map Generation:* The average radius for all ROIs was calculated to ensure that all cells
353 on the tonotopic map had uniform radii. A color key was also generated, with each shade of green
354 representing one frequency. A blank canvas was generated using the Image module from the
355 pillow library, and a circle was created for each cell and filled with the shade of green that
356 represents the cell's best frequency (Barnstedt et al., 2015). Cells that were non-responsive to
357 stimuli were filled in red. The maps from all animals of the same group were aligned together
358 based on the distance from the midline to construct a single map for each group. The tonotopic
359 organization was determined by calculating the correlation between the distance (μm) of every
360 cell from the most medial cell and its best frequency. The significant positive correlation is an
361 indicator of the tonotopic organization when the cells are best tuned to lower and higher
362 frequencies along the medial to the lateral axis. The statistics for the data set, such as the total
363 number of cells, number of responsive cells, and number of non-responsive cells were tallied up
364 and exported in an Excel spreadsheet.

365 *Population Analysis:* The average trace across all GABAergic cells and all non-GABAergic cells
366 was plotted for each frequency and amplitude, similarly to the individual traces. The area under
367 the curve (AUC) was used as a metric for calculation. For every animal, a heat map was generated
368 within each cell type by normalizing all the values across the amplitude/frequency combinations
369 to the highest value. Then one heat map was generated for each exposure group by averaging
370 the normalized values at each amplitude/frequency combination. For every animal, the sound
371 amplitude evokes 20% of the highest response was calculated as a threshold of the activity at
372 each frequency. The (INH/EXC) ratio was calculated by dividing the AUC value of GABAergic

373 cells over that of non-GABAergic cells at each amplitude/frequency combination for each animal
374 across all exposure groups.

375 **Tissue preparation and Western Blot:**

376 *Tissue preparation and protein quantification*

377 Either after the last ABR measurement or immediately after the two-photon imaging, the animals,
378 which were still under anesthesia, were decapitated and their brains were quickly isolated from
379 the skull. The brains were then immediately immersed in isopentane solution, which was pre-cold
380 using dry ice (Ibrahim and Briski, 2014; Alenazi et al., 2015). The frozen brains were then kept in
381 the ultra-cold freezer (-80°C) until further processing. At the time of tissue extraction, the frozen
382 brain was transferred to a cryostat (Leica) at -14° C and left for 5 minutes for equilibration. During
383 this time, one mini tablet of protease and phosphatase Inhibitor (# A32959, Thermo Fisher) was
384 added to 10 ml of ice-cold N-PER Neuronal Protein Extraction Reagent (# 87792, Thermo Fisher)
385 by vigorous vortexing until the tablet was completely dissolved. The brain was then sectioned (50
386 µm) at the level of the IC. For each section that showed the IC, a micro puncher (EMS-Core
387 Sampling, # 50-192-7735, Fisher Scientific) of 1 mm size, was used to dissect the tissue of the
388 whole IC from the two hemispheres. All the dissected tissues from one animal were then dropped
389 into the lysis solution (150 µl), which was then mechanically disrupted using an electrical
390 homogenizer (Polytron, Switzerland). The homogenate was then centrifuged (10,000 x g for 10
391 minutes at 4°C), and the supernatant was then collected leaving the pellets behind. The protein
392 concentration of the supernatant was then determined using Pierce™ BCA Protein Assay Kit (#
393 PI23225, Fisher Scientific) according to the manufacturer's instructions. The supernatant was
394 then kept in the ultra-cold freezer (-80°C) until further processing.

395 *Western Blotting*

396 The protein of the lysates was then adjusted to 20 mg total protein using 4x Laemmli Sample
397 Buffer (#1610747, BIO-RAD). The protein sample was denatured and run on 4-15% Mini-
398 PROTEAN TGX Precast Protein Gels as per the manufacturer's instructions (BIO-RAD). Blots
399 were probed overnight at 4°C with antibodies recognizing GAD67 (1:1000, GAD1 (D1F2M) Rabbit
400 mAb, #41318, Cell Signaling), SOD2 (1:1000, SOD2 (D9V9C) Rabbit mAb, #13194, Cell
401 Signaling) and actin (1:1000, β -Actin Antibody #4967, Cell Signaling). Blots were then processed
402 using anti-rabbit IgG, HRP-linked Antibody (#7074, Cell Signaling) followed by Super Signal West
403 Pico PLUS Chemiluminescent Substrate (#34580, Thermo Fisher) as published before (Ibrahim
404 et al., 2013).

405 **Statistics:**

406 Statistical analysis was done by Origin Pro 2022 software. The litter was the unit of the analysis,
407 and the sex was nested within the litter. One litter from the control group was excluded from the
408 study as the dam of this litter abandoned its pups resulting in the pups' death. Also, not all litters
409 have male and female pups, so the number of litters used in the analysis was different across the
410 exposure groups and sexes. The normality of the data points within each group across the
411 different sexes was examined by the Kolmogorov-Smirnov test. Based on the outcome, the
412 parametric one-way ANOVA and Fisher post hoc tests were used for normal data, while the non-
413 parametric Kruskal-Wallis ANOVA and Donn post hoc tests were used for the non-normal data to
414 examine the significant differences between the exposure groups. A Chi-square test was used to
415 examine the difference between the number of responsive vs. non-responsive cells to sound
416 between each pair of groups. The significant effects were analyzed by the Fisher post hoc test,
417 and the significance was called at $p < 0.05$ for all the statistical tests.

418 **Results**

419 **Developmental exposure to PCBs impairs hearing in male mice.**

420 The toxic effect of developmental exposure to PCBs on hearing has been extensively studied in
421 rats (Goldey et al., 1995; Herr et al., 1996; Crofton and Rice, 1999; Crofton et al., 2000; Lasky et
422 al., 2002; Powers et al., 2006; Kenet et al., 2007; Powers et al., 2009; Sadowski et al., 2016; Lee
423 et al., 2021), which do not provide a rich library of genetically modified models compared to mice.
424 Examination of the toxic interaction between PCBs and noise on different cell types requires a
425 genetically modified model that can aid in cell-type visualization. Therefore, mice were used in
426 this study. To validate the mouse model for PCB studies, we first examined the toxic effect of
427 PCBs on hearing in a mouse model that permits the examination of excitatory and inhibitory cell
428 types. Given that fish are a primary source of PCBs exposure in humans (Persky et al., 2001;
429 Judd et al., 2004; Roveda et al., 2006; Weintraub and Birnbaum, 2008), the Fox River PCB
430 mixture (Sullivan et al., 1983) was used to simulate the human environmental exposure to PCBs.
431 Wild-type female SW mice were daily given a 40-50 mg Nella cookie contaminated with either 0,
432 6, or 12 mg/kg of Fox River PCBs mixture (corn oil based) for 28 days before the breeding with
433 PCBs-unexposed GAD67-GFP knock-in male mice (Tamamaki et al., 2003). Dosing continued
434 throughout pregnancy and lactation until the weaning of their pups. ABR measurements were
435 then taken from the three-month-old offspring to measure their hearing across different PCB
436 developmental exposure levels. Under this experimental paradigm (Fig. 1A), the pre-and
437 postnatal exposure to 6 or 12 mg/kg PCBs produced low-frequency (4 and 8 kHz) hearing
438 impairment compared to vehicle-exposed dams (Fig. 1B), consistent with previous work (Powers
439 et al., 2009). This hearing impairment was only significant in males (Figs. 1C and D). Therefore,
440 only male offspring were selected for further experiments. There was no difference in the hearing
441 threshold of the pups that came from dams either exposed to 6 or 12 mg/kg of PCBs (Fig. 1),
442 which indicated the toxic effect of the PCBs on the hearing of the mice was not dose-dependent
443 within the tested dose range. Therefore, the lower dose (6 mg/kg PCBs mixture) was used for the
444 subsequent experiments.

445 **Developmental exposure to PCB inhibits the recovery from NIHL.**

446 After showing the developmental toxicity of PCB exposure on the hearing of male mice, we next
447 examined the toxic interaction between PCB exposure during development and NIHL in
448 adulthood. An additional cohort of wild-type SW female mice were dosed with 6 mg/kg Fox River
449 PCB mixture daily for 28 days before breeding with PCBs-unexposed GAD67-GFP knock-in male
450 mice and throughout pregnancy and lactation until the weaning of their pups (Fig. 2A). At three
451 months of age, the GFP-positive male pups were randomly divided into two groups: a group
452 exposed to 110 dB SPL broadband noise for 45 minutes (noise-exposed, NE) and a sham group
453 (noise-unexposed, NU). Hence, a total of four subgroups, (Oil/NU, which is the control group of
454 no PCBs or noise exposure), PCB/NU, Oil/NE, and PCB/NE. To measure the baseline hearing,
455 an initial ABR was obtained from all offspring in all groups just before the noise or sham exposure
456 at three months of age. To examine the acute toxic effect of noise exposure, another ABR was
457 taken from all animals immediately after noise exposure (post-noise-day 0). This noise exposure
458 paradigm was selected to induce a temporary threshold shift (Amanipour et al., 2018), so animals
459 would regain their normal hearing one week after the acoustic trauma. Therefore, another ABR
460 was taken from all animals one week after noise exposure (post-noise-day 7) to examine the
461 hearing recovery of the animals after different exposures. Four months later, a final ABR was
462 taken from all animals to assess any aging effect on the hearing baseline of the control group
463 (Oil/NU) as well as the long-term effect of the other exposures on the peripheral auditory system.
464 We observed that all adults that had been exposed to PCB and/or noise showed higher hearing
465 thresholds than those of the control group (Oil/NU) to flat noise (Fig. 2B) and all pure tone
466 frequencies below 24 kHz (Fig. 2C). However, the hearing impairment induced by noise exposure
467 was significantly greater than that induced by PCBs indicated by higher hearing thresholds in
468 Oil/NE or PCB/NE groups than PCB/NU to flat noise and the central frequencies (between 5 and
469 20 kHz) (Fig. 2B and C). Four months after the first ABR measurements, the hearing thresholds
470 to flat noise of all groups did not change from those at day 0, which suggests any aging-related
471 hearing effects across all groups are limited (Fig. 2B). Also, the difference between the thresholds

472 of all groups was similar to the one measured at day 0 (Fig. 2B), which indicates that PCBs and/or
473 noise exposures resulted in long-term permanent damage to the peripheral auditory system.
474 Given the non-significant difference in the hearing threshold between the pups of the (Oil/NE) and
475 (PCB/NE) groups for all tested stimuli (Fig. 2B and C), these data suggest that developmental
476 exposure to a 6 mg/kg Fox River PCBs mixture did not exacerbate the acute effect of NIHL.
477 The hearing recovery under different exposures was assessed by comparing the hearing
478 threshold shift at different time points after noise exposure (Day 0, vs.7, and 120, see Methods).
479 Initially, at day 0 or immediately after the noise exposure, the threshold shift of the animals of both
480 Oil/NE and PCB/NE groups was increased indicating the acute damage of noise exposure to
481 hearing. At day 7 or one week after noise exposure, while the threshold shift of the animals from
482 the Oil/NE group was significantly reduced compared to that at day 0, the threshold shift of the
483 animals from the PCB/NE group remained high indicating that the hearing recovery could be
484 blocked by PCBs. At day 120 or four months after noise exposure, the threshold shift of the
485 animals from the Oil/NE group recovered to be similar to that at day 0 or that of the animals from
486 the PCB/NE group (Fig. 2D). The finding that the threshold shift of the animals from Oil/NE group
487 was increased after hearing recovery suggests that noise exposure could accelerate the cochlear
488 aging as a long-term effect after hearing recovery (Fernandez et al., 2015).
489 Moreover, it was found that the mice that came from dams treated with oil and exposed later to
490 high levels of flat noise (Oil/NE) were able to regain their hearing one week after noise exposure,
491 indicated by a significant reduction of the hearing threshold shift on day 7 compared to day 0 for
492 low-frequency pure tones (5 and 10 kHz) (Fig. 2E). In contrast, developmental exposure to the
493 PCB mixture was found to prevent hearing recovery of the animals exposed later to high-level flat
494 noise (PCB/NE) indicated by the nonsignificant reduction of the hearing threshold shift on day 7
495 compared to that on day 0 for all tested frequencies (Fig. 2E). Consistently, the threshold shift of
496 the pups of the (Oil/NE) group on day 7 was significantly lower than that of the pups of the
497 (PCB/NE) group for the low-frequency pure tones (5 and 10 kHz) (Fig. 2E -). Therefore, the

498 above data suggest that developmental damage of the 6 mg/kg Fox River PCB mixture on hearing
499 at flat noise and lower frequencies impairs the machinery of short-term hearing recovery after
500 noise exposure later in adulthood. However, exposure to high levels of flat noise could accelerate
501 cochlear aging as a long-term effect after hearing recovery.

502 **The effect of PCBs and/or noise exposure on the auditory midbrain**

503 The hyperactivity of the IC was reported after acoustic trauma through many studies (Mulders
504 and Robertson, 2009; Manzoor et al., 2012; Wei 2013; Gröschel et al., 2014), which could be
505 associated with the development of tinnitus as a long-term effect after such acoustic insults, as
506 reviewed (Berger and Coomber, 2015). Therefore, the IC is a good candidate to examine if
507 developmental exposure to PCBs could exacerbate the long-term negative central effects of noise
508 exposure later in adulthood. The IC comprises a major lemniscal division, the central nucleus
509 (ICC), that receives primarily ascending auditory projections (Willard FH and DK, 1983; JF, 2001;
510 DL, 2005), and two non-lemniscal divisions known as the dorsal (DCIC) and lateral (LCIC) cortices
511 that receive massive descending auditory as well as multisensory inputs (Coleman and Clerici,
512 1987; Saldaña et al., 1996; Winer et al., 1998; Bajo and Moore, 2005; Schreiner and Winer, 2005;
513 Loftus et al., 2008; Lesicko et al., 2016; Vaithiyalingam Chandra Sekaran et al., 2021). To
514 examine the differential impact of PCBs on excitatory vs. inhibitory neurons in the IC, and because
515 the IC is superficially accessible in mice (Fig. 3A), two-photon in vivo microscopy was used to
516 monitor the evoked calcium signals of the DCIC neurons to pure tone stimuli. The calcium
517 indicator jRGECO1a was delivered to the non-GABAergic and GABAergic neurons of the DCIC
518 through a viral expression of the red calcium indicator driven by the *Syn* promoter after injecting
519 the DCIC with adeno-associated virus (AAV) immediately after the final ABR measurement (post-
520 noise-day 7). The expression of GFP in the GABAergic neurons of GAD67-GFP knock-in animals
521 enabled us to distinctively monitor the activity of non-GABAergic (GFP-negative) and GABAergic
522 (GFP-positive) neurons. Given that the chronic tinnitus-like behavior can take weeks or months
523 after acoustic trauma to emerge (Longenecker and Galazyuk, 2011; Middleton et al., 2011; Turner

524 et al., 2012), the acoustically evoked neuronal activity was imaged after 28 to 30 weeks of noise
525 exposure to examine any possible long-term central effects. The recording of the evoked calcium
526 signals to different (frequency/amplitude) combinations of pure tones was successfully achieved
527 (Fig. 3B). Based on the best pure tone frequency of each responsive cell (Barnstedt et al., 2015),
528 non-GABAergic and GABAergic cells of the DCIC of the animals from the Oil/NU group showed
529 a similar tonotopic organization reported before (Barnstedt et al., 2015; Wong and Borst, 2019),
530 which consisted of cells tuned to lower and higher frequencies along the rostromedial to the
531 caudolateral axis, respectively. The positive correlation between the distance of each cell on the
532 mediolateral axis and its best frequency is an indicator for the tonotopy shown by the Oil/NU group
533 (Fig. 3C, 1st row). Although PCB/NU and Oil/NE groups showed a significant positive correlation
534 between the distance of the cells along the mediolateral axis and their best frequency indicating
535 a good tonotopic organization over the mediolateral axis, both groups had different profiles of how
536 the best frequencies of the cells are spatially distributed. While the Oil/NE group showed a similar
537 tonotopic map to that of the Oil/NU group featuring some medially located cells tuned to mostly
538 low-frequency pure tones (Fig. 3C: 3rd rows), the PCB/NU group showed a high-low-high map
539 featuring some medially located cells tuned to high-frequency pure tones (Fig. 3C: 2nd row), which
540 was previously reported (Wong and Borst, 2019). This difference in the tonotopic organization of
541 the DCIC neurons across different exposures suggests that the tonotopy of the DCIC could be
542 reshaped based on environmental input. The PCB/NE group showed a complete disruption of
543 tonotopy (Fig. 3C: 4th row) indicated by the lack of a correlation between the distance of the cells
544 along the mediolateral axis and their best frequency. This disruption was characterized by a
545 significant loss of the responsive non-GABAergic cells compared to all other groups (Fig. 3D).
546 This non-responsive zone was mostly located in the lateral areas where the cells were tuned to
547 the higher frequencies (Fig. 3C: 4th row). Consistent with this finding, the distribution of the cells
548 based on best frequency showed a significant low-frequency bias for GABAergic and non-
549 GABAergic neurons in the PCB/NE group compared to all groups (Fig. 3E), which could indicate

550 synaptic reorganization to compensate for the low-frequency hearing loss. A smaller effect was
551 found in the Oil/NE group and PCB/NU groups (Fig. 3E), which could indicate a partial disruption
552 of the DCIC tonotopy. Further, this loss of the neurons tuned to higher frequencies in the lateral
553 areas of the DCIC of the PCB/NE group resulted in a complete reversal of tonotopy (higher to
554 lower frequencies along the medial to the lateral axis) compared to all other groups (lower to
555 higher frequencies along the medial to the lateral axis). However, it is not known if the change in
556 the tonotopic organization of the DCIC is driven by central and/or peripheral components. The
557 significantly higher threshold to flat noise of the animals from PCB/NU, Oil/NE, and PCB/NE
558 groups at the time of the two-photon imaging compared to that of the control (Oil/NU) group (Fig.
559 2B) suggests that the changes in the DCIC induced by different exposures could be due to
560 peripheral damage. Although PCB/NE and Oil/NE groups shared a similar threshold to the flat
561 noise 4 months after noise exposure (Fig. 2B), PCB/NE group had a disrupted tonotopy compared
562 to that shown by the Oil/NE group, which indicates that the DCIC changes induced by PCBs and
563 noise exposure (PCB/NE) was accompanied by central changes.

564 Compared to the Oil/NU group, both PCB/NU and Oil/NE groups had more responsive GABAergic
565 and non-GABAergic neurons to pure tone stimuli (Fig. 3C: 2nd and 3rd rows & Fig. 3D), which could
566 indicate an increased gain induced by homeostatic plasticity after the peripheral damage and
567 consistent with the previous finding showing the increased gain of the corticocollicular axons
568 reported after noise-induced hearing loss (Asokan et al., 2018). To test this possibility, the
569 average cellular response across all tested frequencies and amplitudes was calculated based on
570 the AUC of the evoked response. Consistent with our hypothesis, there was an increase in the
571 evoked cellular response of non-GABAergic and GABAergic cells of the Oil/NE and PCB/NU
572 groups compared to control (Oil/NU) (Non-GABAergic cells: Kruskal-Wallis ANOVA, $\chi^2= 183.6$, p
573 $= 1.49 \times 10^{-39}$, post hoc Dunn's Test: $p = 1.5 \times 10^{-10}$ or 5.1×10^{-7} for Oil/NE (Median = 270 .7) or
574 PCB/NU (Median = 274.8) vs.Oil/NU (Median = 210.6), respectively & GABAergic cells: Kruskal-
575 Wallis ANOVA, $\chi^2= 66.7$, $p = 2.2 \times 10^{-14}$, post hoc Dunn's Test: $p = 1.7 \times 10^{-7}$ or 4.7×10^{-6} for

576 Oil/NE (Median = 211 .5) or PCB/NU (Median = 228.9) vs.Oil/NU (Median = 105.2), respectively),
577 indicating a higher gain of both cell types in Oil/NE and PCB/NU groups. In contrast, the response
578 of non-GABAergic cells only of the PCB/NE group was reduced compared to the control (Non-
579 GABAergic cells: Kruskal-Wallis ANOVA, $\chi^2= 183.6$, $p = 1.49 \times 10^{-39}$, post hoc Dunn's Test: $p =$
580 1.95×10^{-7} for PCB/NE (Median = 142) vs.Oil/NU (Median = 210.6) & GABAergic cells: Kruskal-
581 Wallis ANOVA, $\chi^2= 66.7$, $p = 2.2 \times 10^{-14}$, post hoc Dunn's Test: $p = 1.0$ for PCB/NE (Median =
582 112.96) vs.Oil/NU (Median = 105.2)), suggesting that the combination between PCBs and noise
583 exposure did not induce a synaptic compensatory mechanism to the peripheral damage. These
584 results suggest that the cellular gain could be modulated based on the degree of the peripheral
585 or central damage induced by different exposures in a frequency-dependent manner. Within the
586 population of responsive neurons of the DCIC to sound in the unexposed control animals (Oil/NU),
587 it was found that 27.5% and 18.3% of responsive non-GABAergic and GABAergic cells,
588 respectively, could be activated by sound at 40 dB SPL. Therefore, we asked if a sound at 40 dB
589 SPL could activate a similar percentage of cells in the DCIC of Oil/NE (hearing recovered)
590 vs.PCB/NE (hearing unrecovered). Whereas a similar percentage of non-GABAergic and
591 GABAergic cells could be activated by a 40 dB SPL sound level in the Oil/NE compared to the
592 Oil/NU group (Fig. 3F: 27.6% and 23.3% of responsive non-GABAergic and GABAergic cells,
593 respectively), a significantly lower percentage of cells were activated by a 40 dB sound level in
594 the PCB/NE group (Fig. 3F: 2.4% and 0.0% of responsive non-GABAergic and GABAergic cells,
595 respectively). By interpolation, the PCB/NE group was found to require a higher sound level (53.8
596 and 52.6 dB SPL) to activate a similar fraction of the responsive non-GABAergic and GABAergic
597 cells, respectively (Fig. 3F) as the Oil/NU group, which was consistent with the persistent toxic
598 effect of PCBs that prevented the hearing recovery. Consistent with the hearing damage induced
599 by PCB exposure, the DCIC cells of PCB/NU showed a significantly lower fraction of activated
600 non-GABAergic cells by a 40 dB SPL sound level compared to those of the Oil/NU group (Fig.

601 3F: 8.0% and 9.4% of responsive non-GABAergic and GABAergic cells, respectively) and then
602 required a moderately higher sound level (47.6 and 42.5 dB SPL) to activate a similar percentage
603 of non-GABAergic and GABAergic cells, respectively, compared to the Oil/NU group (Fig. 3F). In
604 addition, all groups showed a similar fraction of activated cells at a 60 dB SPL sound level,
605 suggesting that most differences were seen at relatively low sound pressure levels (Fig. 3F). The
606 above data show that the combination of developmental exposure to PCBs and noise exposure
607 in adulthood had a significant long-term negative impact on the DCIC neurons, which is
608 characterized by a disruption of the tonotopic organization and an increase of the threshold of
609 DCIC neurons.

610 **The effect of PCBs and/or noise exposure on the inhibition and excitation balance of the**
611 **DCIC.**

612 For each amplitude/frequency combination, the pooled AUC values of the calcium signals
613 obtained from either non-GABAergic or GABAergic cells were calculated to examine excitatory or
614 inhibitory activities, respectively, of the DCIC across different exposures. After normalizing the
615 AUC values against the highest value across all amplitude/frequency combinations per each
616 animal, a heat map was made by averaging the AUC values across all animals in each group.
617 The visual assessment of these maps indicated that the frequency response areas (FRAs) in the
618 exposure groups (PCB/NU, Oil/NE, and PCB/NE) were smaller compared to the control group
619 (Oil/NU). To quantify this difference, the sound level evoking 20% of the highest response at each
620 frequency was assigned as a sound threshold at that frequency for each animal within each group.
621 Compared to the control group, all animals exposed to either PCBs, noise, or their combination
622 required a significantly higher sound pressure level to get a 20% of response at 10 and 14.1 kHz
623 for non-GABAergic cells and GABAergic cells (Fig. 4B and C, Table 4). The PCB-exposed
624 animals either those exposed to PCBs alone or PCBs combined with noise required a significantly
625 higher sound level to achieve 20% activity of their GABAergic cells at 28.3 kHz (Fig. 4C, Table
626 4). As indicated by the visual assessment of the heat maps, the FRA of inhibitory or GABAergic

627 cells of the PCB/NE group was smaller than that of the control group (Oil/NU), which indicated a
628 loss of inhibition induced by PCB exposure. Given that this loss of inhibition could be associated
629 with a loss of excitation of a similar degree, the inhibition/excitation (INH/EXC) ratio was computed
630 to examine the occurrence of inhibitory downregulation. The (INH/EXC) ratio was calculated by
631 dividing the pooled AUC values of GABAergic by those of non-GABAergic cells at either each
632 sound amplitude across different frequencies or at each sound frequency across different
633 amplitudes. Although the (INH/EXC) ratio was not significantly different between all groups at all
634 sound amplitudes (Fig. 4D), the (INH/EXC) ratio of all exposure groups was significantly lower
635 than that of the control group (Oil/NU) at 5 kHz (Fig. 4E). In addition, the combination of PCBs
636 and noise exposure (PCB/NE) resulted in a persistent low (INH/EXC) ratio at 7.1 kHz compared
637 to the control group (Oil/NU). Also, the noise-exposed groups had a lower (INH/EXC) ratio than
638 that of (PCB/NU) at 7.1 kHz (Fig. 4E). These data suggest that PCBs, noise, or their combination
639 could manipulate the activity of the DCIC in a frequency-dependent manner. For instance, at
640 higher frequencies (10-14 kHz), the PCBs and/or noise exposure increase the threshold of both
641 excitatory and inhibitory activities in a balanced manner indicated by no change in the (INH/EXC)
642 ratio. In contrast, the PCBs and/or noise exposure disrupted the balance between inhibition and
643 excitation by downregulating the inhibition at 5 kHz with no change in the activity threshold.
644 However, only the combination of PCBs and noise exposure extended the inhibitory
645 downregulation at 7.1 kHz.

646 **The association between the downregulation of inhibition and oxidative stress.**

647 Given that both PCB and noise exposure are associated with high levels of oxidative stress
648 (Spreng, 2000; Samson et al., 2008; Bavithra et al., 2012; Lee et al., 2012; Selvakumar et al.,
649 2012; Daiber et al., 2020; Mao and Chen, 2021; McCann et al., 2021), it was important to examine
650 the capacity of the animals developmentally exposed to PCBs and/or noise in adulthood to
651 mitigate oxidative stress. Therefore, the brains of the animals across different exposures were
652 isolated at different time points (three months of age after the last ABR measurement which was

653 post-noise-day 7 and seven months of age after the two-photon imaging). The brains were frozen
654 and sectioned at the level of the IC. Then, multiple 1 mm biopsies were taken from the IC structure
655 using a micro-puncture (Fig. 5A). The tissue specimens were processed for Western Blot to
656 examine the levels of the metabolic enzyme sodium dismutase-2 (SOD2), which is one of the
657 important enzymes that function to scavenge reactive oxygen species (ROS) (Fig. 5B). Although
658 the levels of SOD2 showed no significant differences between the exposure groups, low SOD2
659 levels were found in older animals of higher body weight that were exposed to PCBs and/or noise
660 indicated by a significant negative correlation between the SOD2 levels and the age or the body
661 weight of the animals. This effect was stronger in the PCB/NE group (Figs. 5C and D). This finding
662 was consistent with many reports showing that aging or higher body weight could induce higher
663 levels of oxidative stress that could be associated with lower levels of SOD2 (Pansarasa et al.,
664 1999; Tatone et al., 2006; Zeng et al., 2014; Balasubramanian et al., 2020). Moreover, consistent
665 with the strong correlation between noise exposure and high levels of oxidative stress, low SOD2
666 levels were associated with higher hearing threshold values in the Oil/NE group only (Fig. 5E).

667 GABAergic cells are known for their vulnerability to oxidative stress (as reviewed (Ibrahim and
668 Llano, 2019)), so we asked if the downregulation of inhibition induced by PCBs and noise
669 exposure is associated with high levels of oxidative stress. Therefore, the tissue specimens were
670 processed for Western Blot to examine the levels of glutamate acid decarboxylase-67 (GAD67),
671 which is the main cytosolic enzyme to produce GABA as an indicator for the level of inhibition,
672 and SOD2 (Fig. 5B). Initially, the GAD67 levels showed no significant difference between the
673 exposure groups, which was consistent with the previous report (Bandara et al., 2016). However,
674 only the PCB/NE group showed a significant positive correlation between GAD67 and SOD2 (Fig.
675 5F) suggesting that GABAergic inhibition was retained in animals with a higher capacity to clear
676 the ROS, which may suggest that at least part of the downregulation of inhibition seen after PCB
677 and noise exposure may be related to an increase in oxidative stress in the IC.

678 **Discussion:**

679 The current study shows that developmental exposure to PCBs resulted in a sex-dependent low-
680 frequency hearing loss in mice, that pre- and perinatal PCB exposure prevented the normal
681 recovery of hearing after adult noise exposure, that PCB and noise exposure leads to
682 downregulation of synaptic inhibition and disruption of tonotopy of the IC, and that this
683 downregulation of inhibition may be related to increases in oxidative stress. Thus, this work
684 provides a new mechanistic understanding of how an environmentally common combination of
685 toxins leads to central changes in the auditory system and how developmental toxin exposure
686 can have long-lasting neural consequences. Below we address the technical considerations and
687 implications of this work.

688 ***Technical considerations and comparison with previous work:***

689 The female mice exposed to PCBs and the breeding GAD67-GFP knock-in male mice share the
690 same SW background. The SW is a well-known outbred strain that has generally good hearing
691 into young adulthood (Zheng et al., 1999). Consistent with that, the control animals showed no
692 change in their hearing threshold throughout the study (7 months of age) (Fig. 2B) indicating
693 limited aging or genetic-related negative effects on hearing during the study. A relatively short
694 duration/high intensity noise exposure paradigm was used in this study. This paradigm was used
695 because previous work had shown that rats developmentally exposed to PCBs developed
696 audiogenic seizures (AGS) after they were exposed to higher sound pressure levels (Poon et al.,
697 2015; Bandara et al., 2016). Therefore, in our paradigm, mice were anesthetized during noise
698 exposure, which limits the activity of the middle ear reflex (MER), which is known for its protective
699 role against acoustic damage (Brask, 1979; Deiters et al., 2019). Thus, the particular noise
700 exposure protocol here was more likely to cause hearing loss than in awake animals, as reflected
701 in the increased hearing thresholds seen in this study.

702 Two-photon imaging of the IC was conducted under ketamine anesthesia. As a well-known
703 anesthetic, ketamine has been used in some studies showing the large-scale tonotopic
704 organization in the mouse auditory cortex (Stiebler et al., 1997; Linden et al., 2003; Guo et al.,

705 2012; Yudintsev et al., 2021), which showed a similar topographical functional organization under
706 ketamine and awake state (Guo et al., 2012). However, ketamine may broaden the bandwidth of
707 the FRA and lengthen the response duration (Guo et al., 2012), which could impact the tonal
708 selectivity and temporal properties of the responses. Also, ketamine was reported to increase the
709 spontaneous activity of the IC cells in guinea pigs (Astl et al., 1996; Syka et al., 2000) and the
710 auditory cortex of the rats, which resulted in trial-to-trial variability (Kisley and Gerstein, 1999). To
711 correct for such variability between runs, the average response of all runs across the tested
712 amplitudes at each frequency was taken. The same procedures were followed across all exposure
713 groups.

714 Our results showed that the difference between the hearing thresholds and impact of PCB
715 exposure in phase 2 (Fig. 2C) was larger than that found in phase 1 (Fig. 1C) across the tested
716 frequencies. The cause of these cohort-effects are not known, though similar cohort effects have
717 been seen in previous developmental PCB exposure work (Lee et al., 2021). In the current study,
718 phase 1 and phase 2 were performed one year apart with separate outbred SW breeders
719 purchased for each phase, suggesting that genetic variability may contribute to these differences
720 (Cui et al., 1993). The differences seen in the two cohorts reinforce the need to use matched
721 cohorts for PCB-based studies, particularly in outbred strains. However, despite these
722 differences, the trends seen in both cohorts are highly consistent with previous studies
723 establishing PCB effects on hearing (Goldey et al., 1995; Crofton and Rice, 1999; Crofton et al.,
724 2000; Powers et al., 2006; Powers et al., 2009).

725 Our results showed that the low INH/EXC ratio found in PCB/NE observed via two-photon imaging
726 was associated with no change in the expression level of GAD67 across all groups, while the
727 previous study done on rats (Bandara et al., 2016) showed a decrease in IC GAD expression
728 after PCB exposure. Such contradictory results could be explained by the difference in the
729 experimental sampling and scaling. While the two-photon imaging was done on the DCIC, the
730 whole IC tissue was dissected for protein quantification due to the technical difficulty to obtain a

731 pure representative sample of the DCIC. Therefore, the results obtained by each technique could
732 implicate sub-region-specific changes in IC after the acoustic trauma. Consistent with that notion,
733 and indicated by the click-evoked potentials measured from the external cortex of the IC and its
734 central nucleus after acoustic trauma, it was found that the responses of the two IC sub-regions
735 are different (Szczepaniak and Møller, 1996). Such differences could originate from the difference
736 in input and output between the lemniscal (Willard FH and DK, 1983; JF, 2001; DL, 2005) and
737 non-lemniscal (Coleman and Clerici, 1987; Saldaña et al., 1996; Winer et al., 1998; Bajo and
738 Moore, 2005; Schreiner and Winer, 2005; Loftus et al., 2008) regions of the IC.

739 ***Implications***

740 *PCBs, hearing, and sex differences:*

741 Our data are consistent with multiple previous studies demonstrating that developmental PCB
742 exposure causes hearing loss (Goldey et al., 1995; Herr et al., 1996; Crofton and Rice, 1999;
743 Crofton et al., 2000; Lasky et al., 2002; Powers et al., 2006; Kenet et al., 2007; Powers et al.,
744 2009). Several hypotheses exist to explain the impact of developmental PCB exposure on
745 hearing. First, the toxic effect of PCBs on the thyroid gland leads to developmental alteration to
746 the cochlea (Uziel, 1986; Goldey et al., 1995; Goldey and Crofton, 1998; Knipper et al., 2000;
747 Song et al., 2008). Other studies showed the direct toxicity of PCBs on the development of the
748 cochlea by allowing elevations of intracellular calcium concentration in the outer hair cells via
749 ryanodine receptors (Wong et al., 1997; Bobbin, 2002; Sziklai, 2004). Our data also showed that
750 the PCBs and/or noise exposure was associated with long-term permanent damage to hearing,
751 which seemed to be uniquely driven by those exposures without aging-related effects at least four
752 months after acoustic trauma or seven months of age, which is consistent with other reports
753 showing hearing impairment at relevant time points (Powers et al., 2009; Liu et al., 2018). Also,
754 the data showed that noise exposure can accelerate aging associated hearing loss after short-
755 term hearing recovery, which was consistent with previous work (Fernandez et al., 2015).

756 Regarding the sex-dependent toxic effect of PCB exposure, previous studies reported that
757 developmental exposure to PCBs showed mixed sex-dependent effects on behavior, locomotion,
758 and vision in rats (Kremer et al., 1999; Geller et al., 2001; Vega-López et al., 2007; Cauli et al.,
759 2013; Bell et al., 2016). Here, low-frequency hearing loss induced by developmental exposure to
760 PCBs was only shown in male offspring. This finding could implicate the possible protective role
761 of estrogen against hearing loss. For example, postmenopausal women were found to have a
762 higher ABR threshold compared to younger women or men (Wharton and Church, 1990). Similar
763 increases in thresholds were found in ovariectomized rats compared to the controls (Coleman et
764 al., 1994). Estrogen was also found to have a protective effect against cochlear injury, gentamicin
765 ototoxicity, noise, or age-related hearing loss (Nakamagoe et al., 2010; Tabuchi et al., 2011;
766 Caras, 2013; Milon et al., 2018).

767 *PCBs, noise, and the central auditory system:*

768 In addition to its negative impact on the peripheral auditory system, many studies examined the
769 central effects of developmental exposure to PCBs or NIHL. The reduction of GABAergic inhibition
770 (Poon et al., 2015; Bandara et al., 2016; Lee et al., 2021) and tonotopic reorganization (Kenet et
771 al., 2007; Izquierdo et al., 2008; Pienkowski and Eggermont, 2009) are the most central common
772 effects of PCBs and noise exposure. Consistent with previous reports, the DCIC of control animals
773 showed a tonotopic map of non-GABAergic and GABAergic cells along the mediolateral axis
774 (Barnstedt et al., 2015; Wong and Borst, 2019). Although similar distributions of responsive cells
775 were seen after PCB exposure or noise exposure, there were more responsive cells to sound
776 than control (Figs. 3C and D), which could be due to compensatory plasticity (Wang et al., 1996;
777 Mulders and Robertson, 2009; Niu et al., 2013; Auerbach et al., 2014; Asokan et al., 2018). After
778 PCB or noise exposure, the tuning frequencies of the cells were biased toward low frequencies
779 (Fig. 3E), which could represent a compensatory mechanism in response to low-frequency
780 hearing loss. In addition, the disruption of the tonotopic organization of the DCIC following the
781 combination of PCBs and noise exposure involved both non-GABAergic and GABAergic cell

782 populations. This tonotopic disruption was characterized by low responsiveness to sound and a
783 possibility of reversed tonotopy of cells. The lower fraction of the responsive cells to sound in the
784 PCB/NE group was only significant within the non-GABAergic neuronal population compared to
785 the control group, which could indicate a selective synaptic mechanism targeting those cells. Our
786 data are consistent with previous work showing that the PCB exposure disrupts the tonotopy of
787 the primary AC, which was characterized by a non-responsive zone to sound or a reversed
788 tonotopy (Kenet et al., 2007). Given that different exposure groups had higher hearing thresholds
789 compared to the control at the time of two-photon imaging (4 months after noise exposure), the
790 changes in the DCIC could be related to peripheral hearing loss, which is well-established to
791 cause changes at the level of the IC (Ma et al., 2006; Izquierdo et al., 2008; Mulders and
792 Robertson, 2011; Manzoor et al., 2012; Gröschel et al., 2014; Heeringa and van Dijk, 2014; Vogler
793 et al., 2014). However, noise-exposed animals with or without PCBs exposure had similar hearing
794 thresholds at the time of imaging, while the DCIC of the PCB/NE group showed a disrupted
795 tonotopic organization. These data suggest that collicular changes induced by the combination
796 between PCBs and noise exposure lead to central reorganization independent of peripheral
797 hearing loss. For instance, the presence of tonotopic disruption at the level of the midbrain
798 suggests that disruption in the AC may be inherited from lower centers. Alternatively, given the
799 massive feedback to the DCIC from the AC (Asilador and Llano, 2020; Vaithiyalingam Chandra
800 Sekaran et al., 2021; Yuditsev et al., 2021), the tonotopic disruption observed in the current
801 study could be related to disrupted top-down corticocollicular inputs. Future work will be needed
802 to sort out these possibilities.

803 *PCBs, noise, GABA, and oxidative stress:*

804 PCB exposure in rats was associated with audiogenic seizures, which were associated with the
805 downregulation of the inhibition indicated by the lower levels of the GAD56 enzyme (Bandara et
806 al., 2016). Also, the NIHL causes neural hyperactivity in the central auditory system as reviewed
807 (Zhao et al., 2016). Therefore, it was important to examine the balance between excitation and

808 inhibition following PCBs exposure and/or noise exposure. The current study demonstrated that
809 the PCB/NE group showed the smallest FRA for inhibitory neurons. It was also found that all PCB-
810 exposed animals and/or high-level noise required a higher sound level to reach 20% of its
811 response in both GABAergic and non-GABAergic cell populations. Moreover, a lower INH/EXC
812 ratio was shown by all exposure groups at 5 kHz and by PCB/NE at 7.1 kHz, which suggests that
813 the disruption of the balance between the excitation and inhibition by those exposures could be
814 frequency-dependent. These results were supported by previous findings of PCB-induced
815 disruption of the dynamics between the excitatory and inhibitory neurotransmission in the AC
816 (Kenet et al., 2007; Lee et al., 2021). At the level of the IC, PCBs exposure was found to decrease
817 the inhibition by reducing the level of GAD65 expression (Bandara et al., 2016). In addition, noise-
818 induced hearing loss was found to disrupt the balance between inhibition and excitation in the IC
819 and AC in mice (Scholl and Wehr, 2008; Roberts et al., 2010; Wang et al., 2011; Sturm et al.,
820 2017).

821 Many GABAergic cells lack adequate defense mechanisms against oxidative stress (Ibrahim and
822 Llano, 2019), which makes them more vulnerable to oxidative stress compared to other types of
823 neurons. Given that PCBs and noise exposure are linked with an increase in oxidative and
824 metabolic stress (McCann et al., 2021) (Pessah et al., 2019; Daiber et al., 2020; Liu et al., 2020),
825 the downregulation of inhibition could be associated with a higher level of oxidative stress. The
826 IC is among the most metabolically active regions in the brain (Landau et al., 1955; Sokoloff,
827 1981; Gross et al., 1987; Zeller et al., 1997; Bordia and Zahr, 2020). Therefore, we examined the
828 association between the downregulation of inhibition and the oxidative stress indicated by the
829 expression levels of both GAD67 and SOD2, respectively. As expected, the exposure to PCBs
830 and/or noise promoted a positive correlation between oxidative stress, as indicated by the high
831 levels of SOD2, and age and weight gain, which was consistent with previous reports (Pansarasa
832 et al., 1999; Tatone et al., 2006; Zeng et al., 2014; Balasubramanian et al., 2020). Despite the
833 absence of change in the level of both GAD67 and SOD2 levels across groups, a positive

834 correlation between GAD67 and SOD2 expression was found in the PCB/NE group only,
835 suggesting that GABAergic inhibition was retained in animals with a higher capacity to clear ROS.
836 Indeed, future studies will be required to investigate the expression levels of different components
837 involved in GABA production and/or function such as GAD65, which was reported to be reduced
838 by PCB exposure in rats (Bandara et al., 2016), and GABA receptors. In addition, regional
839 heterogeneity to oxidative stress, possibly related to perineuronal net expression, may lead to
840 differential sensitivity to PCBs and noise based on the IC subregion (Schofield and Beebe, 2019).

841 *Interactions between PCBs and noise exposure:*

842 Most of the effects of combined exposure to PCBs and noise were not entirely predictable by the
843 effects of exposure to either PCBs or noise individually. For example, PCBs and noise exposure
844 appear to combine nonlinearly to produce peripheral hearing loss. This interaction is evidenced
845 by the finding that developmental exposure to PCBs did not exacerbate acute NIHL, but it
846 prevented hearing recovery after one week of the acoustic trauma (Figure 2). Centrally at the level
847 of the DCIC, while the individual exposures to PCBs or noise increased the number of responsive
848 cells and their gain, the combined exposure to PCBs and noise reversed those effects (Fig. 3F).
849 However, some linear interactions were also shown. These nonlinear interactions emphasize the
850 need to conduct studies that examine the impact of both individual and combined toxin exposure
851 on the developing auditory system.

852 In conclusion, developmental exposure to PCBs was found to impair the hearing of the male
853 offspring of PCB-treated mouse dams and to prevent hearing recovery after acoustic trauma.
854 PCBs exposure and noise exposure resulted in the disruption of the tonotopic map of the DCIC
855 that was characterized by a wide non-responsive zone to sound, reversed, and low-frequency-
856 biased tonotopy. Such effects were associated with the disruption of the excitation and inhibition
857 balance via the downregulation of inhibition at lower frequencies and associated with diminished
858 capacity to reduce oxidative stress. Given the level of PCBs still present in the environment, and
859 the high (and growing) incidence of low-level noise exposure in our society (Beyer and Biziuk,

860 2009; Flamme et al., 2012; Lie et al., 2016; Weber et al., 2018), the current data in combination
861 with previous work suggest that the auditory consequences of these exposures are likely
862 widespread, synergistic, sex-dependent and involve disruption to broad areas of the central
863 auditory system. Future work will be needed to understand the mechanisms by which these
864 changes occur so that approaches may be designed to mitigate the damage caused by these
865 common environmental toxicants.

866

867

868

869 **Figure legends**

870 **Figure 1. Developmental exposure to PCBs impairs hearing in male mice.**

871 **A**, The timeline of the experimental design of the PCB dosing of dams and hearing assessment
872 of the pups. **B**, A line plot of the hearing threshold across different frequencies for all pups came
873 from dams under different exposures (One-Way ANOVA: $f(2,33) = 6.1$, $p = 0.005$, Fisher post
874 hoc test: $*p = 0.002$ and 0.007 for Oil vs. 6 and 12 mg/kg PCB, respectively, and $p = 0.58$ for 6
875 vs. 12 mg/kg PCB at 4 kHz & $f(2,33) = 10.8$, $*p = 2.4 \times 10^{-4}$ and 7.1×10^{-5} for Oil vs. 6 and 12 mg/kg
876 PCB, respectively, and $p = 0.28$ for 6 vs. 12 mg/kg PCB at 8 kHz & $f(2,32) = 3.1$, $p = 0.06$ at 16 kHz
877 & $f(2,26) = 1.2$, $p = 0.31$ at 24 kHz). **C**, A line plot of the hearing threshold across different
878 frequencies for male pups came from dams under different exposures (One-Way ANOVA: $f(2,16)$
879 $= 8.3$, $p = 0.003$, Fisher post hoc test: $*p = 9.1 \times 10^{-4}$ and 0.01 for Oil vs. 6 and 12 mg/kg PCB,
880 respectively, and $p = 0.19$ for 6 vs. 12 mg/kg PCB at 4 kHz & $f(2,16) = 5.5$, $p = 0.02$, Fisher post
881 hoc test: $*p = 0.02$ and 0.005 for Oil vs. 6 and 12 mg/kg PCB, respectively, and $p = 0.43$ for 6 vs.
882 12 mg/kg PCB at 8 kHz & $f(2,15) = 2.0$, $p = 0.17$ at 16 kHz & $f(2,11) = 1.1$, $p = 0.36$ at 24 kHz). **D**, A
883 line plot of the hearing threshold across different frequencies for female pups came from dams
884 under different exposures (One-Way ANOVA: $f(2,14) = 1.1$, $p = 0.36$ at 4 kHz & $f(2,13) = 3.2$, $p =$
885 0.08 at 8 kHz & $f(2,14) = 1.1$, $p = 0.35$ at 16 kHz & $f(2,14) = 0.4$, $p = 0.67$ at 24 kHz). *: The significance
886 against Oil treated group.

887 **Figure 2. Developmental exposure to PCB inhibits the recovery from NIHL.**

888 **A**, The timeline of the experimental design of the PCBs dosing of dams, the overexposure to the
889 noise of the pups, and hearing assessment of the pups before or after noise overexposure. **B**, A
890 bar graph showing the threshold to flat noise under different exposures across two-time points
891 (Day 0 and 120) (One-Way ANOVA: $f(7, 76) = 14.3$, $p = 9.6 \times 10^{-12}$, Fisher post hoc test: $*p = 0.009$,
892 2.8×10^{-7} , or 2.1×10^{-8} for Oil/NU vs. PCB/NU, Oil/NE, or PCB/NE, respectively, at day 0 & $*p =$
893 0.03 , 9.3×10^{-6} , or 3.9×10^{-7} for Oil/NU vs. PCB/NU, Oil/NE, or PCB/NE, respectively, at day 120 &

894 #p = 4.8×10^{-4} or $0.7.1 \times 10^{-5}$ for PCB/NU vs. Oil/NE or PCB/NE, respectively, at day 0 & #p = 0.03
895 or 0.005 for PCB/NU vs. Oil/NE or PCB/NE, respectively, at day 120 & p = 0.74 and 0.48 for
896 Oil/NE vs. PCB/NE at day 0 and 120, respectively & p = 0.45, 0.24, 0.57, 0.30 for day 0 vs. 120
897 at Oil/NU, PCB/NU, Oil/NE, and PCB/NE, respectively). **C**, A line graph of the ABR threshold to
898 pure tones from different exposure groups (At 5 kHz, One-Way ANOVA: $f_{(3, 36)} = 8.7$, $p = 1.8 \times 10^{-4}$,
899 Fisher post hoc test: *p = 0.004, 1.6×10^{-4} , or 5.2×10^{-5} for Oil/NU vs. PCB/NU, Oil/NE, or PCB/NE,
900 respectively & p = 0.19 for PCB/NU vs. Oil/NE, 0.11 for PCB/NU vs. PCB/NE, and 0.79 for Oil/NE
901 vs. PCB/NE, (At 10 kHz, One-Way ANOVA: $f_{(3, 36)} = 11.4$, $p = 2.0 \times 10^{-5}$, Fisher post hoc test: *p =
902 0.005, 5.0×10^{-5} , or 4.6×10^{-6} for Oil/NU vs. PCB/NU, Oil/NE, or PCB/NE, respectively & #p = 0.02
903 PCB/NU vs. PCB/NE & p = 0.08 for PCB/NU vs. Oil/NE and 0.63 for Oil/NE vs PCB/NE), (At 14
904 kHz, One-Way ANOVA: $f_{(3, 36)} = 15.1$, $p = 1.6 \times 10^{-6}$, Fisher post hoc test: *p = 0.02, 4.0×10^{-6} , or
905 1.2×10^{-6} for Oil/NU vs. PCB/NU, Oil/NE, or PCB/NE, respectively & #p = 0.04 or 0.002 for PCB/NU
906 vs. Oil/NE or PCB/NE, respectively & p = 0.81 for Oil/NE vs. PCB/NE), (At 16 kHz, One-Way
907 ANOVA: $f_{(3, 34)} = 12.6$, $p = 1.1 \times 10^{-5}$, Fisher post hoc test: *p = 0.003, 1.7×10^{-5} , or 3.5×10^{-6} for
908 Oil/NU vs. PCB/NU, Oil/NE, or PCB/NE, respectively & #p = 0.04 or 0.02 for PCB/NU vs. Oil/NE or
909 PCB/NE, respectively & p = 0.81 for Oil/NE vs. PCB/NE), (At 20 kHz, One-Way ANOVA: $f_{(3, 36)} =$
910 11.8, $p = 1.6 \times 10^{-5}$, Fisher post hoc test: *p = 0.002, 1.4×10^{-5} , or 7.6×10^{-6} for Oil/NU vs. PCB/NU,
911 Oil/NE, or PCB/NE, respectively & p = 0.08 for PCB/NU vs. Oil/NE, 0.06 for PCB/NU vs. PCB/NE,
912 and 0.94 for Oil/NE vs. PCB/NE), and (At 24 kHz, Kruskal-Wallis ANOVA, $\chi^2 = 9.04$, $p = 0.03$, post
913 hoc Dunn's Test: p = 1.0, 0.22, and 0.41 for Oil/NU vs. PCB/NU, Oil/NE, and PCB/NE,
914 respectively, and p = 1.0 for all remaining comparisons). **D**, A bar graph of the hearing threshold
915 shift to the flat noise immediately, a week, or 4 months after acoustic trauma for the pups from
916 dams exposed to PCBs or Oil (PCB/NE vs. Oil/NE) (One-Way ANOVA: $f_{(5, 38)} = 4.4$, $p = 0.002$,
917 Fisher post hoc test: ^ap = 0.003, p = 0.42, and ^bp = 8.3×10^{-4} for day 0 vs. 7, day 0 vs. 120, and
918 day 7 vs. 120, respectively, at Oil/NE & p = 0.58, 0.15, and 0.06 for day 0 vs. 7, day 0 vs. 120,
919 and day 7 vs. 120, respectively, at PCB/NE & p = 0.85, ^sp = 0.03, and p = 0.63 for Oil/NE vs

920 PCB/NE at day 0, 7, and 120, respectively). **E**, A line graph of the hearing threshold shift to
921 different pure tone frequencies immediately or a week after acoustic trauma for the pups from
922 dams exposed to PCBs or Oil (PCB/NE vs.Oil/NE) (At 5 kHz, One-Way ANOVA: $f_{(3, 32)} = 7.3$, $p =$
923 7.0×10^{-4} , Fisher post hoc test: $*p = 1.5 \times 10^{-4}$ and $p = 0.32$ for day 0 vs.7 at Oil/NE and PCB/NE,
924 respectively & $\#p = 0.007$ for PCB/NE vs.Oil/NE at day 7), (At 10 kHz, One-Way ANOVA: $f_{(3, 32)} =$
925 4.9 , $p = 0.007$, Fisher post hoc test: $*p = 0.002$ and $p = 0.39$ for day 0 vs.7 at Oil/NE and PCB/NE,
926 respectively & $\#p = 0.02$ for PCB/NE vs.Oil/NE at day 7), and (One-Way ANOVA: $f_{(3, 32)} = 1.7$, p
927 $= 0.19$ at 14 kHz, $f_{(3, 32)} = 0.94$, $p = 0.42$ at 16 kHz, $f_{(3, 32)} = 0.17$, $p = 0.9$ at 20 kHz, and $f_{(3, 32)} =$
928 0.51 , $p = 0.67$ at 24 kHz). The exposure groups are plotted as Oil/NU: black, PCB/NU: red, Oil/NE:
929 blue, and PCB/NE: purple; *: The significance against (Oil/NU) group; #: The significance against
930 (PCB/NU) group; §: The significance against (Oil/NE) group, ^a: The significance against day 0,
931 and ^b: The significance against day 120.

932 **Figure 3. The effect of PCBs and/or noise exposure on the DCIC cells.**

933 **A**, A brightfield image of the surface of the DCIC. **B**, The time traces of the evoked calcium
934 signals by different stimuli of pure tones obtained from non-GABAergic (top) and GABAergic
935 (bottom) cells of the DCIC imaged from the surface; The length and the color of the gradient
936 green bars indicate the intensity and the frequency of the stimulus, respectively. **C**, Pseudocolor
937 images show the activity of the cells on the DCIC across different animals from (Oil/NU: 1st row,
938 PCB/NU: 2nd row, Oil/NE: 3rd row, and PCB/NE: 4th row) in response to the pure tone based on
939 their best frequency as graded green circles for the responsive cells and solid red circles for the
940 non-responsive cells (Pearson Corr. 0.69 ($p = 2.4 \times 10^{-37}$), 0.56 ($p = 2.6 \times 10^{-37}$), 0.7 ($p = 6.5 \times 10^{-$
941 69), and -0.007 ($p = 0.92$) for non-GABAergic cells of Oil/NU, PCB/NU, Oil/NE, and PCB/NE,
942 respectively & Pearson Corr. 0.63 ($p = 1.9 \times 10^{-6}$), 0.56 ($p = 3.7 \times 10^{-13}$), 0.62 ($p = 5.6 \times 10^{-17}$), and -
943 0.03 ($p = 0.85$) for GABAergic cells of Oil/NU, PCB/NU, Oil/NE, and PCB/NE, respectively). **D**, A
944 heat map showing the fraction of the responsive non-GABAergic (left) (Chi-square test: $\chi^2 = 227$

945 (*p <0.001), 111 (*p <0.001) and 9.9 (*p = 0.001) for Oil/NE vs.PCB/NU, Oil/NE, and PCB/NE,
946 respectively & $\chi^2= 36.3$ (#p <0.001) and 311 (#p <0.001) for PCB/NU vs.Oil/NE and PCB/NE,
947 respectively & $\chi^2= 181$ (§p <0.001) for Oil/NE vs.PCB/NE) and GABAergic (right) (Chi-square
948 test: $\chi^2= 79.8$ (*p <0.001), 54.6 (*p <0.001) and 0.09 (p = 0.67) for Oil/NE vs.PCB/NU, Oil/NE,
949 and PCB/NE, respectively & $\chi^2= 4.2$ (#p = 0.04) and 65.2 (#p <0.001) for PCB/NU vs.Oil/NE and
950 PCB/NE, respectively & $\chi^2= 42$ (§p <0.001) for Oil/NE vs.PCB/NE) cells to sounds across all
951 exposure groups. **E**, A cumulative distribution function for non-GABAergic (left) (Kruskal-Wallis
952 ANOVA: $\chi^2= 156$, *p <0.001 for Oil/NE vs.PCB/NU, Oil/NE, and PCB/NE, respectively & #p =
953 0.003 and #p = 7.1×10^{-7} for PCB/NU vs.Oil/NE and PCB/NE, respectively & §p <0.001 for Oil/NE
954 vs.PCB/NE) and GABAergic (right) (Kruskal-Wallis ANOVA: $\chi^2= 59.9$, *p = 5.0×10^{-6} , *p = $4.2 \times 10^{-$
955 4 , *p <0.001 for Oil/NE vs.PCB/NU, Oil/NE, and PCB/NE, respectively & p = 1.0 and #p = $5.5 \times 10^{-$
956 5 for PCB/NU vs.Oil/NE and PCB/NE, respectively & §p = 7.0×10^{-7} for Oil/NE vs.PCB/NE) cells of
957 the DCIC based on their best frequency. **F**, A line graph showing the fraction of evoked non-
958 GABAergic (left) (Chi-square test: $\chi^2= 53.3$ (*p <0.001), $\chi^2= 0.0043$ (p = 0.99), and 43.6 (#p
959 <0.001) for Oil/NU vs. PCB/NU, Oil/NE, and PCB/NE, respectively, at 40 dB SPL & $\chi^2= 0.06$ (p
960 = 0.99), $\chi^2= 0.34$ (p = 0.95), and 0.52 (p = 0.91) for Oil/NU vs. PCB/NU, Oil/NE, and PCB/NE,
961 respectively, at 60 dB SPL) and GABAergic (right) (Chi-square test: $\chi^2= 3.7$ (p = 0.29), $\chi^2= 0.65$
962 (p = 0.88), and $\chi^2= 9.9$ (*p = 0.02) for Oil/NU vs. PCB/NU, Oil/NE, and PCB/NE at 40 dB SPL &
963 $\chi^2= 0.42$ (p = 0.92), $\chi^2= 5.1$ (p = 0.16), and 0.001 (p = 0.99) for Oil/NU vs. PCB/NU, Oil/NE, and
964 PCB/NE, respectively, at 60 dB SPL) cells of the DCIC at each sound level within the
965 responsive cell population across all exposure groups; The exposure groups are plotted as
966 Oil/NU: black line, PCB/NU: red line, Oil/NE: blue line, and PCB/NE: purple line; *The
967 significance against (Oil/NU) group; #The significance against (PCB/NU) group; §The
968 significance against (Oil/NE) group; Cereb: Cerebellum; CTx: Cortex, DCIC: dorsal cortex of the

969 inferior colliculus, TS: The transverse sinus. A rainbow color code was selected for different
970 frequencies, N.R in grey: Non-responsive cells.

971 **Figure 4. The effect of PCBs and/or noise exposure on the inhibition and excitation balance**
972 **of the DCIC.**

973 **A**, Heat maps showing the excitatory (left) and inhibitory (right) average response across the
974 animals of each exposure group (Oil/NU: 1st row, PCB/NU: 2nd row, Oil/NE: 3rd row, and PCB/NE:
975 4th row). **B-C**, Line graphs showing the sound level required to evoke 20% of the sound response
976 in non-GABAergic (One way ANOVA: At 10 kHz, $f_{(3, 20)} = 9.0$, $p = 5.7 \times 10^{-4}$, Fisher post hoc test:
977 $*p = 0.0002$, 0.002 , and 0.0002 for Oil/NU vs. PCB/NU, Oil/NE, and PCB/NE, respectively, $p = 0.2$
978 for PCB/NU vs. Oil/NE, 0.79 for PCB/NU vs. PCB/NE, and 0.28 for Oil/NE vs. PCB/NE & at 14.1
979 kHz, $f_{(3, 20)} = 8.0$, $p = 0.001$, Fisher post hoc test: $*p = 0.004$, 0.008 , and 0.0001 for Oil/NU
980 vs. PCB/NU, Oil/NE, and PCB/NE, respectively, $p = 0.62$ for PCB/NU vs. Oil/NE, 0.18 for PCB/NU
981 vs. PCB/NE, and 0.06 for Oil/NE vs. PCB/NE & $f_{(3, 20)} = 0.24$, $p = 0.86$ at 5kHz, $f_{(3, 20)} = 0.53$, $p =$
982 0.67 at 7.1 kHz, $f_{(3, 20)} = 1.7$, $p = 0.19$ at 20 kHz, $f_{(3, 20)} = 2.3$, $p = 0.1$ at 28.3 kHz, and $f_{(3, 20)} =$
983 0.75 , $p = 0.35$ at 40 kHz) or GABAergic (One way ANOVA: At 10 kHz, $f_{(3, 20)} = 6.9$, $p = 0.002$,
984 Fisher post hoc test: $*p = 0.006$, 0.02 , and 0.0003 for Oil/NU vs. PCB/NU, Oil/NE, and PCB/NE,
985 respectively, $p = 0.49$ for PCB/NU vs. Oil/NE, 0.29 for PCB/NU vs. PCB/NE, and 0.07 for Oil/NE
986 vs. PCB/NE & at 14.1 kHz, $f_{(3, 20)} = 6.9$, $p = 0.002$, Fisher post hoc test: $*p = 0.01$, 0.01 , and
987 0.0002 for Oil/NU vs. PCB/NU, Oil/NE, and PCB/NE, respectively, $p = 0.78$ for PCB/NU vs. Oil/NE,
988 0.16 for PCB/NU vs. PCB/NE, and 0.08 for Oil/NE vs. PCB/NE & at 28.3 kHz, $f_{(3, 20)} = 3.3$, $p =$
989 0.04 , Fisher post hoc test: $*p = 0.02$, $p = 0.06$ and $*p = 0.01$ for Oil/NU vs. PCB/NU, Oil/NE, and
990 PCB/NE, respectively, $p = 0.46$ for PCB/NU vs. Oil/NE, 0.92 for PCB/NU vs. PCB/NE, and 0.37
991 for Oil/NE vs. PCB/NE & $f_{(3, 20)} = 1.1$, $p = 0.38$ at 5kHz, $f_{(3, 20)} = 1.1$, $p = 0.36$ at 7.1 kHz, $f_{(3, 20)} =$
992 1.6 , $p = 0.23$ at 20 kHz, $f_{(3, 20)} = 0.75$, $p = 0.35$ at 40 kHz) cells, respectively, across different pure
993 tone frequencies for each group. **D-E**, Line graphs showing the inhibition/excitation ratio across

994 different amplitudes or frequencies (One way ANOVA: At 5 kHz, $f_{(3, 18)} = 4.9$, $p = 0.01$, Fisher post
995 hoc test: $*p = 0.037$, 0.039 , and 0.001 for Oil/NU vs.PCB/NU, Oil/NE, and PCB/NE, respectively,
996 $p = 0.73$ for PCB/NU vs. Oil/NE, 0.23 for PCB/NU vs. PCB/NE, and 0.09 for Oil/NE vs. PCB/NE
997 & at 7.1 kHz, $f_{(3, 16)} = 5.4$, $p = 0.009$, Fisher post hoc test: $*p = 0.01$ for Oil/NU vs.PCB/NU, $\#p =$
998 0.02 and 0.003 for PCB/NU vs.Oil/NE and PCB/NE, respectively, $p = 0.47$ for Oil/NU vs. PCB/NU,
999 0.06 for Oil/NU vs. Oil/NE, and 0.24 for Oil/NE vs. PCB/NE & $f_{(3, 19)} = 1.8$, $p = 0.18$ at 10kHz, $f_{(3,$
1000 $19)} = 1.4$, $p = 0.27$ at 14.1 kHz, $f_{(3, 18)} = 0.36$, $p = 0.78$ at 20 kHz, $f_{(3, 17)} = 1.4$, $p = 0.29$ at 28.3 kHz,
1001 and $f_{(3, 17)} = 1.3$, $p = 0.30$ at 40 kHz), respectively, of pure tone stimulus for each exposure group;
1002 The exposure groups are plotted as Oil/NU: black line, PCB/NU: red line, Oil/NE: blue line, and
1003 PCB/NE: purple line; $*$ The significance against (Oil/NU) group; $\#$ The significance against
1004 (PCB/NU) group.

1005 **Figure 5. The association between the downregulation of inhibition and oxidative stress.**

1006 **A**, A cartoon image showing the process of tissue collection and gel running for Western Blot
1007 (Some features were taken from <https://biorender.com>). **B**, An image showing the Western Blots
1008 of GAD67 (1st row), actin (2nd row), and SOD2 (3rd row). **C-F**, Line graphs showing the
1009 correlation between the normalized expression levels of the SOD2 enzyme and either age, body
1010 weight, or the normalized expression level of the GAD67 enzyme for the (PCB/NE) group as
1011 well as ABR for the (Oil/NE) group. $*$: p-values for each correlation.

1012 **Acknowledgments:**

1013 The authors deeply thank the National Institute of Environmental Health Sciences (NIEHS) for
1014 funding this work under the NIH Postdoctoral trainee in Endocrine, Developmental & Reproductive
1015 Toxicology (T32 ES007326) , the National Institute on Deafness and other Communication
1016 Disorders (R01 DC016599) and the NIH Office of Research Infrastructure Programs (S10
1017 OD023569).

1018 **References:**

- 1019 Abbott SD, Hughes LF, Bauer CA, Salvi R, Caspary DM (1999) Detection of glutamate decarboxylase
1020 isoforms in rat inferior colliculus following acoustic exposure. *Neuroscience* 93:1375-1381.
- 1021 Akerboom J et al. (2012) Optimization of a GCaMP calcium indicator for neural activity imaging. *J*
1022 *Neurosci* 32:13819-13840.
- 1023 Alenazi FSH, Ibrahim BA, Briski KP (2015) Estradiol Regulates Dorsal Vagal Complex Signal Transduction
1024 Pathway Transcriptional Reactivity to the AMPK Activator 5-Aminoimidazole-4-Carboxamide-
1025 Riboside (AICAR). *J Mol Neurosci* 56:907-916.
- 1026 Amanipour RM, Zhu X, Duvey G, Celanire S, Walton JP, Frisina RD (2018) Noise-Induced Hearing Loss in
1027 Mice: Effects of High and Low Levels of Noise Trauma in CBA Mice. *Conf Proc IEEE Eng Med Biol*
1028 *Soc* 2018:1210-1213.
- 1029 Asilador A, Llano DA (2020) Top-Down Inference in the Auditory System: Potential Roles for Corticofugal
1030 Projections. *Front Neural Circuits* 14:615259.
- 1031 Asokan MM, Williamson RS, Hancock KE, Polley DB (2018) Sensory overamplification in layer 5 auditory
1032 corticofugal projection neurons following cochlear nerve synaptic damage. *Nat Commun* 9:2468.
- 1033 Astl J, Popelár J, Kvasnák E, Syka J (1996) Comparison of response properties of neurons in the inferior
1034 colliculus of guinea pigs under different anesthetics. *Audiology* 35:335-345.
- 1035 Auerbach BD, Rodrigues PV, Salvi RJ (2014) Central gain control in tinnitus and hyperacusis. *Front Neurol*
1036 5:206.
- 1037 Bajo VM, Moore DR (2005) Descending projections from the auditory cortex to the inferior colliculus in
1038 the gerbil, *Meriones unguiculatus*. *J Comp Neurol* 486:101-116.
- 1039 Balasubramanian P, Asirvatham-Jeyaraj N, Monteiro R, Sivasubramanian MK, Hall D, Subramanian M
1040 (2020) Obesity-induced sympathoexcitation is associated with Nrf2 dysfunction in the rostral
1041 ventrolateral medulla. *Am J Physiol Regul Integr Comp Physiol* 318:R435-R444.
- 1042 Bandara SB, Eubig PA, Sadowski RN, Schantz SL (2016) Developmental PCB Exposure Increases
1043 Audiogenic Seizures and Decreases Glutamic Acid Decarboxylase in the Inferior Colliculus.
1044 *Toxicol Sci* 149:335-345.
- 1045 Barnstedt O, Keating P, Weissenberger Y, King AJ, Dahmen JC (2015) Functional Microarchitecture of the
1046 Mouse Dorsal Inferior Colliculus Revealed through In Vivo Two-Photon Calcium Imaging. *J*
1047 *Neurosci* 35:10927-10939.
- 1048 Bavithra S, Selvakumar K, Pratheepa Kumari R, Krishnamoorthy G, Venkataraman P, Arunakaran J (2012)
1049 Polychlorinated biphenyl (PCBs)-induced oxidative stress plays a critical role on cerebellar
1050 dopaminergic receptor expression: ameliorative role of quercetin. *Neurotox Res* 21:149-159.
- 1051 Bell MR, Hart BG, Gore AC (2016) Two-hit exposure to polychlorinated biphenyls at gestational and
1052 juvenile life stages: 2. Sex-specific neuromolecular effects in the brain. *Mol Cell Endocrinol*
1053 420:125-137.
- 1054 Berger JI, Coomber B (2015) Tinnitus-related changes in the inferior colliculus. *Front Neurol* 6:61.
- 1055 Bergström B, Nyström B (1986) Development of hearing loss during long-term exposure to occupational
1056 noise. A 20-year follow-up study. *Scand Audiol* 15:227-234.
- 1057 Beyer A, Biziuk M (2009) Environmental fate and global distribution of polychlorinated biphenyls. *Rev*
1058 *Environ Contam Toxicol* 201:137-158.
- 1059 Bobbin RP (2002) Caffeine and ryanodine demonstrate a role for the ryanodine receptor in the organ of
1060 Corti. *Hear Res* 174:172-182.
- 1061 Bordia T, Zahr NM (2020) The Inferior Colliculus in Alcoholism and Beyond. *Front Syst Neurosci*
1062 14:606345.
- 1063 Brask T (1979) The noise protection effect of the stapedius reflex. *Acta Otolaryngol Suppl* 360:116-117.

- 1064 Brouwer A, Longnecker MP, Birnbaum LS, Cogliano J, Kostyniak P, Moore J, Schantz S, Winneke G (1999)
1065 Characterization of potential endocrine-related health effects at low-dose levels of exposure to
1066 PCBs. *Environ Health Perspect* 107 Suppl 4:639-649.
- 1067 Cadot S, Frenz D, Maconochie M (2012) A novel method for retinoic acid administration reveals
1068 differential and dose-dependent downregulation of Fgf3 in the developing inner ear and
1069 anterior CNS. *Dev Dyn* 241:741-758.
- 1070 Caras ML (2013) Estrogenic modulation of auditory processing: a vertebrate comparison. *Front*
1071 *Neuroendocrinol* 34:285-299.
- 1072 Cauli O, Piedrafita B, Llansola M, Felipo V (2013) Gender differential effects of developmental exposure
1073 to methyl-mercury, polychlorinated biphenyls 126 or 153, or its combinations on motor activity
1074 and coordination. *Toxicology* 311:61-68.
- 1075 Coleman JR, Clerici WJ (1987) Sources of projections to subdivisions of the inferior colliculus in the rat. *J*
1076 *Comp Neurol* 262:215-226.
- 1077 Coleman JR, Campbell D, Cooper WA, Welsh MG, Moyer J (1994) Auditory brainstem responses after
1078 ovariectomy and estrogen replacement in rat. *Hear Res* 80:209-215.
- 1079 Crofton KM, Rice DC (1999) Low-frequency hearing loss following perinatal exposure to 3,3',4,4',5-
1080 pentachlorobiphenyl (PCB 126) in rats. *Neurotoxicol Teratol* 21:299-301.
- 1081 Crofton KM, Ding D, Padich R, Taylor M, Henderson D (2000) Hearing loss following exposure during
1082 development to polychlorinated biphenyls: a cochlear site of action. *Hear Res* 144:196-204.
- 1083 Cui S, Chesson C, Hope R (1993) Genetic variation within and between strains of outbred Swiss mice. *Lab*
1084 *Anim* 27:116-123.
- 1085 Daiber A, Kröller-Schön S, Oelze M, Hahad O, Li H, Schulz R, Steven S, Münzel T (2020) Oxidative stress
1086 and inflammation contribute to traffic noise-induced vascular and cerebral dysfunction via
1087 uncoupling of nitric oxide synthases. *Redox Biol* 34:101506.
- 1088 Dana H, Mohar B, Sun Y, Narayan S, Gordus A, Hasseman JP, Tsegaye G, Holt GT, Hu A, Walpita D, Patel
1089 R, Macklin JJ, Bargmann CI, Ahrens MB, Schreiter ER, Jayaraman V, Looger LL, Svoboda K, Kim DS
1090 (2016) Sensitive red protein calcium indicators for imaging neural activity. *Elife* 5.
- 1091 Daniell WE, Swan SS, McDaniel MM, Camp JE, Cohen MA, Stebbins JG (2006) Noise exposure and
1092 hearing loss prevention programmes after 20 years of regulations in the United States. *Occup*
1093 *Environ Med* 63:343-351.
- 1094 Deiters KK, Flamme GA, Tasko SM, Murphy WJ, Greene NT, Jones HG, Ahroon WA (2019) Generalizability
1095 of clinically measured acoustic reflexes to brief sounds. *J Acoust Soc Am* 146:3993.
- 1096 Ding T, Yan A, Liu K (2019) What is noise-induced hearing loss? *Br J Hosp Med (Lond)* 80:525-529.
- 1097 DL O (2005) Neuronal organization in the inferior colliculus. In: *The inferior colliculus*. (JA W, CE S, eds),
1098 pp 69–114. New York: Springer.
- 1099 Dong S, Rodger J, Mulders WH, Robertson D (2010a) Tonotopic changes in GABA receptor expression in
1100 guinea pig inferior colliculus after partial unilateral hearing loss. *Brain Res* 1342:24-32.
- 1101 Dong S, Mulders WH, Rodger J, Woo S, Robertson D (2010b) Acoustic trauma evokes hyperactivity and
1102 changes in gene expression in guinea-pig auditory brainstem. *Eur J Neurosci* 31:1616-1628.
- 1103 Fernandez KA, Jeffers PW, Lall K, Liberman MC, Kujawa SG (2015) Aging after noise exposure:
1104 acceleration of cochlear synaptopathy in "recovered" ears. *J Neurosci* 35:7509-7520.
- 1105 Fitzgerald EF, Hwang SA, Bush B, Cook K, Worswick P (1998) Fish consumption and breast milk PCB
1106 concentrations among Mohawk women at Akwesasne. *Am J Epidemiol* 148:164-172.
- 1107 Fitzgerald EF, Brix KA, Deres DA, Hwang SA, Bush B, Lambert G, Tarbell A (1996) Polychlorinated biphenyl
1108 (PCB) and dichlorodiphenyl dichloroethylene (DDE) exposure among Native American men from
1109 contaminated Great Lakes fish and wildlife. *Toxicol Ind Health* 12:361-368.
- 1110 Flamme GA, Stephenson MR, Deiters K, Tatro A, van Gessel D, Geda K, Wyllys K, McGregor K (2012)
1111 Typical noise exposure in daily life. *Int J Audiol* 51 Suppl 1:S3-11.

- 1112 Geller AM, Oshiro WM, Haykal-Coates N, Kodavanti PR, Bushnell PJ (2001) Gender-dependent
1113 behavioral and sensory effects of a commercial mixture of polychlorinated biphenyls (Aroclor
1114 1254) in rats. *Toxicol Sci* 59:268-277.
- 1115 Giovannucci A, Friedrich J, Gunn P, Kalfon J, Brown BL, Koay SA, Taxidis J, Najafi F, Gauthier JL, Zhou P,
1116 Khakh BS, Tank DW, Chklovskii DB, Pnevmatikakis EA (2019) CalmAn an open source tool for
1117 scalable calcium imaging data analysis. *Elife* 8.
- 1118 Goldey ES, Crofton KM (1998) Thyroxine replacement attenuates hypothyroxinemia, hearing loss, and
1119 motor deficits following developmental exposure to Aroclor 1254 in rats. *Toxicol Sci* 45:94-105.
- 1120 Goldey ES, Kehn LS, Lau C, Rehnberg GL, Crofton KM (1995) Developmental exposure to polychlorinated
1121 biphenyls (Aroclor 1254) reduces circulating thyroid hormone concentrations and causes
1122 hearing deficits in rats. *Toxicol Appl Pharmacol* 135:77-88.
- 1123 Goldey GJ, Roumis DK, Glickfeld LL, Kerlin AM, Reid RC, Bonin V, Schafer DP, Andermann ML (2014)
1124 Removable cranial windows for long-term imaging in awake mice. *Nat Protoc* 9:2515-2538.
- 1125 Gross PM, Sposito NM, Pettersen SE, Panton DG, Fenstermacher JD (1987) Topography of capillary
1126 density, glucose metabolism, and microvascular function within the rat inferior colliculus. *J*
1127 *Cereb Blood Flow Metab* 7:154-160.
- 1128 Gröschel M, Ryll J, Götze R, Ernst A, Basta D (2014) Acute and long-term effects of noise exposure on the
1129 neuronal spontaneous activity in cochlear nucleus and inferior colliculus brain slices. *Biomed Res*
1130 *Int* 2014:909260.
- 1131 Guo W, Chambers AR, Darrow KN, Hancock KE, Shinn-Cunningham BG, Polley DB (2012) Robustness of
1132 cortical topography across fields, laminae, anesthetic states, and neurophysiological signal
1133 types. *J Neurosci* 32:9159-9172.
- 1134 Guo YL, Lambert GH, Hsu CC, Hsu MM (2004) Yucheng: health effects of prenatal exposure to
1135 polychlorinated biphenyls and dibenzofurans. *Int Arch Occup Environ Health* 77:153-158.
- 1136 Heeringa AN, van Dijk P (2014) The dissimilar time course of temporary threshold shifts and reduction of
1137 inhibition in the inferior colliculus following intense sound exposure. *Hear Res* 312:38-47.
- 1138 Herr DW, Goldey ES, Crofton KM (1996) Developmental exposure to Aroclor 1254 produces low-
1139 frequency alterations in adult rat brainstem auditory evoked responses. *Fundam Appl Toxicol*
1140 33:120-128.
- 1141 Ibrahim BA, Briski KP (2014) Role of dorsal vagal complex A2 noradrenergic neurons in hindbrain
1142 glucoprivic inhibition of the luteinizing hormone surge in the steroid-primed ovariectomized
1143 female rat: effects of 5-thioglucoase on A2 functional biomarker and AMPK activity. *Neuroscience*
1144 269:199-214.
- 1145 Ibrahim BA, Llano DA (2019) Aging and Central Auditory Disinhibition: Is It a Reflection of Homeostatic
1146 Downregulation or Metabolic Vulnerability? *Brain Sci* 9.
- 1147 Ibrahim BA, Tamrakar P, Gujar AD, Cherian AK, Briski KP (2013) Caudal fourth ventricular administration
1148 of the AMPK activator 5-aminoimidazole-4-carboxamide-riboside regulates glucose and
1149 counterregulatory hormone profiles, dorsal vagal complex metabolosensory neuron function,
1150 and hypothalamic Fos expression. *J Neurosci Res* 91:1226-1238.
- 1151 Izquierdo MA, Gutiérrez-Conde PM, Merchán MA, Malmierca MS (2008) Non-plastic reorganization of
1152 frequency coding in the inferior colliculus of the rat following noise-induced hearing loss.
1153 *Neuroscience* 154:355-369.
- 1154 Jacobson JL, Fein GG, Jacobson SW, Schwartz PM, Dowler JK (1984) The transfer of polychlorinated
1155 biphenyls (PCBs) and polybrominated biphenyls (PBBs) across the human placenta and into
1156 maternal milk. *Am J Public Health* 74:378-379.
- 1157 JF W (2001) Handbook of mouse auditory research. In: Behavior to molecular biology (JF W, ed). Boca
1158 Raton, FL: CRC.

- 1159 Judd N, Griffith WC, Faustman EM (2004) Contribution of PCB exposure from fish consumption to total
1160 dioxin-like dietary exposure. *Regul Toxicol Pharmacol* 40:125-135.
- 1161 Jusko TA, Sisto R, Iosif AM, Moleti A, Wimmerová S, Lancz K, Tihányi J, Sovčíková E, Drobná B,
1162 Palkovičová L, Jurečková D, Thevenet-Morrison K, Verner MA, Sonneborn D, Hertz-Picciotto I,
1163 Trnovec T (2014) Prenatal and postnatal serum PCB concentrations and cochlear function in
1164 children at 45 months of age. *Environ Health Perspect* 122:1246-1252.
- 1165 Kenet T, Froemke RC, Schreiner CE, Pessah IN, Merzenich MM (2007) Perinatal exposure to a
1166 noncoplanar polychlorinated biphenyl alters tonotopy, receptive fields, and plasticity in rat
1167 primary auditory cortex. *Proc Natl Acad Sci U S A* 104:7646-7651.
- 1168 Kisley MA, Gerstein GL (1999) Trial-to-trial variability and state-dependent modulation of auditory-
1169 evoked responses in cortex. *J Neurosci* 19:10451-10460.
- 1170 Knipper M, Zinn C, Maier H, Praetorius M, Rohbock K, Köpschall I, Zimmermann U (2000) Thyroid
1171 hormone deficiency before the onset of hearing causes irreversible damage to peripheral and
1172 central auditory systems. *J Neurophysiol* 83:3101-3112.
- 1173 Knipper M, Singer W, Schwabe K, Hagberg GE, Li Hegner Y, Rüttiger L, Braun C, Land R (2021) Disturbed
1174 Balance of Inhibitory Signaling Links Hearing Loss and Cognition. *Front Neural Circuits*
1175 15:785603.
- 1176 Kostyniak PJ, Hansen LG, Widholm JJ, Fitzpatrick RD, Olson JR, Helferich JL, Kim KH, Sable HJ, Seegal RF,
1177 Pessah IN, Schantz SL (2005) Formulation and characterization of an experimental PCB mixture
1178 designed to mimic human exposure from contaminated fish. *Toxicol Sci* 88:400-411.
- 1179 Kremer H, Lilienthal H, Hany J, Roth-Härer A, Winneke G (1999) Sex-dependent effects of maternal PCB
1180 exposure on the electroretinogram in adult rats. *Neurotoxicol Teratol* 21:13-19.
- 1181 LANDAU WM, FREYGANG WH, ROLAND LP, SOKOLOFF L, KETY SS (1955) The local circulation of the living
1182 brain; values in the unanesthetized and anesthetized cat. *Trans Am Neurol Assoc*:125-129.
- 1183 Lasky RE, Widholm JJ, Crofton KM, Schantz SL (2002) Perinatal exposure to Aroclor 1254 impairs
1184 distortion product otoacoustic emissions (DPOAEs) in rats. *Toxicol Sci* 68:458-464.
- 1185 Lee CM, Sadowski RN, Schantz SL, Llano DA (2021) Developmental PCB Exposure Disrupts Synaptic
1186 Transmission and Connectivity in the Rat Auditory Cortex, Independent of Its Effects on
1187 Peripheral Hearing Threshold. *eNeuro* 8.
- 1188 Lee DW, Notter SA, Thiruchelvam M, Dever DP, Fitzpatrick R, Kostyniak PJ, Cory-Slechta DA, Opanashuk
1189 LA (2012) Subchronic polychlorinated biphenyl (Aroclor 1254) exposure produces oxidative
1190 damage and neuronal death of ventral midbrain dopaminergic systems. *Toxicol Sci* 125:496-508.
- 1191 Lesicko AM, Hristova TS, Maigler KC, Llano DA (2016) Connectional Modularity of Top-Down and
1192 Bottom-Up Multimodal Inputs to the Lateral Cortex of the Mouse Inferior Colliculus. *J Neurosci*
1193 36:11037-11050.
- 1194 Lie A, Skogstad M, Johannessen HA, Tynes T, Mehlum IS, Nordby KC, Engdahl B, Tambs K (2016)
1195 Occupational noise exposure and hearing: a systematic review. *Int Arch Occup Environ Health*
1196 89:351-372.
- 1197 Linden JF, Liu RC, Sahani M, Schreiner CE, Merzenich MM (2003) Spectrotemporal structure of receptive
1198 fields in areas AI and AAF of mouse auditory cortex. *J Neurophysiol* 90:2660-2675.
- 1199 Liu J, Tan Y, Song E, Song Y (2020) A Critical Review of Polychlorinated Biphenyls Metabolism,
1200 Metabolites, and Their Correlation with Oxidative Stress. *Chem Res Toxicol* 33:2022-2042.
- 1201 Liu L, Xuan C, Shen P, He T, Chang Y, Shi L, Tao S, Yu Z, Brown RE, Wang J (2018) Hippocampal
1202 Mechanisms Underlying Impairment in Spatial Learning Long After Establishment of Noise-
1203 Induced Hearing Loss in CBA Mice. *Front Syst Neurosci* 12:35.
- 1204 Loftus WC, Malmierca MS, Bishop DC, Oliver DL (2008) The cytoarchitecture of the inferior colliculus
1205 revisited: a common organization of the lateral cortex in rat and cat. *Neuroscience* 154:196-205.

- 1206 Longenecker RJ, Galazyuk AV (2011) Development of tinnitus in CBA/CaJ mice following sound exposure.
1207 J Assoc Res Otolaryngol 12:647-658.
- 1208 Ma WL, Hidaka H, May BJ (2006) Spontaneous activity in the inferior colliculus of CBA/J mice after
1209 manipulations that induce tinnitus. Hear Res 212:9-21.
- 1210 Manzoor NF, Licari FG, Klapchar M, Elkin RL, Gao Y, Chen G, Kaltenbach JA (2012) Noise-induced
1211 hyperactivity in the inferior colliculus: its relationship with hyperactivity in the dorsal cochlear
1212 nucleus. J Neurophysiol 108:976-988.
- 1213 Mao H, Chen Y (2021) Noise-Induced Hearing Loss: Updates on Molecular Targets and Potential
1214 Interventions. Neural Plast 2021:4784385.
- 1215 McCann MS, Fernandez HR, Flowers SA, Maguire-Zeiss KA (2021) Polychlorinated biphenyls induce
1216 oxidative stress and metabolic responses in astrocytes. Neurotoxicology 86:59-68.
- 1217 Middleton JW, Kiritani T, Pedersen C, Turner JG, Shepherd GM, Tzounopoulos T (2011) Mice with
1218 behavioral evidence of tinnitus exhibit dorsal cochlear nucleus hyperactivity because of
1219 decreased GABAergic inhibition. Proc Natl Acad Sci U S A 108:7601-7606.
- 1220 Milon B, Mitra S, Song Y, Margulies Z, Casserly R, Drake V, Mong JA, Depireux DA, Hertzano R (2018) The
1221 impact of biological sex on the response to noise and otoprotective therapies against acoustic
1222 injury in mice. Biol Sex Differ 9:12.
- 1223 Min JY, Kim R, Min KB (2014) Serum polychlorinated biphenyls concentrations and hearing impairment
1224 in adults. Chemosphere 102:6-11.
- 1225 Morse DC, Wehler EK, Wesseling W, Koeman JH, Brouwer A (1996) Alterations in rat brain thyroid
1226 hormone status following pre- and postnatal exposure to polychlorinated biphenyls (Aroclor
1227 1254). Toxicol Appl Pharmacol 136:269-279.
- 1228 Mulders WH, Robertson D (2009) Hyperactivity in the auditory midbrain after acoustic trauma:
1229 dependence on cochlear activity. Neuroscience 164:733-746.
- 1230 Mulders WH, Robertson D (2011) Progressive centralization of midbrain hyperactivity after acoustic
1231 trauma. Neuroscience 192:753-760.
- 1232 Nakamagoe M, Tabuchi K, Uemaetomari I, Nishimura B, Hara A (2010) Estradiol protects the cochlea
1233 against gentamicin ototoxicity through inhibition of the JNK pathway. Hear Res 261:67-74.
- 1234 Niu Y, Kumaraguru A, Wang R, Sun W (2013) Hyperexcitability of inferior colliculus neurons caused by
1235 acute noise exposure. J Neurosci Res 91:292-299.
- 1236 Palkovičová Murínová Ľ, Moleti A, Sisto R, Wimmerová S, Jusko TA, Tihányi J, Jurečková D, Kováč J,
1237 Koštiaková V, Drobná B, Trnovec T (2016) PCB exposure and cochlear function at age 6 years.
1238 Environ Res 151:428-435.
- 1239 Pansarasa O, Bertorelli L, Vecchiet J, Felzani G, Marzatico F (1999) Age-dependent changes of
1240 antioxidant activities and markers of free radical damage in human skeletal muscle. Free Radic
1241 Biol Med 27:617-622.
- 1242 Persky V, Turyk M, Anderson HA, Hanrahan LP, Falk C, Steenport DN, Chatterton R, Freels S, Consortium
1243 GL (2001) The effects of PCB exposure and fish consumption on endogenous hormones. Environ
1244 Health Perspect 109:1275-1283.
- 1245 Pessah IN, Lein PJ, Seegal RF, Sagiv SK (2019) Neurotoxicity of polychlorinated biphenyls and related
1246 organohalogenes. Acta Neuropathol 138:363-387.
- 1247 Pienkowski M, Eggermont JJ (2009) Long-term, partially-reversible reorganization of frequency tuning in
1248 mature cat primary auditory cortex can be induced by passive exposure to moderate-level
1249 sounds. Hear Res 257:24-40.
- 1250 Pnevmatikakis EA, Giovannucci A (2017) NoRMCorre: An online algorithm for piecewise rigid motion
1251 correction of calcium imaging data. J Neurosci Methods 291:83-94.
- 1252 Poon E, Bandara SB, Allen JB, Sadowski RN, Schantz SL (2015) Developmental PCB exposure increases
1253 susceptibility to audiogenic seizures in adulthood. Neurotoxicology 46:117-124.

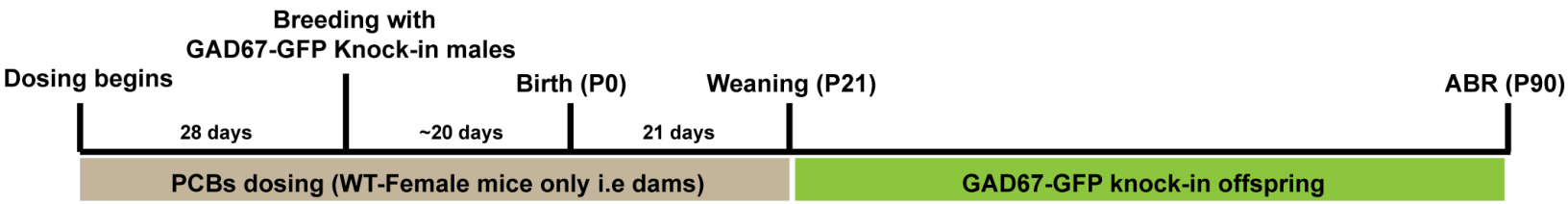
- 1254 Powers BE, Widholm JJ, Lasky RE, Schantz SL (2006) Auditory deficits in rats exposed to an
1255 environmental PCB mixture during development. *Toxicol Sci* 89:415-422.
- 1256 Powers BE, Poon E, Sable HJ, Schantz SL (2009) Developmental exposure to PCBs, MeHg, or both: long-
1257 term effects on auditory function. *Environ Health Perspect* 117:1101-1107.
- 1258 Roberts LE, Eggermont JJ, Caspary DM, Shore SE, Melcher JR, Kaltenbach JA (2010) Ringing ears: the
1259 neuroscience of tinnitus. *J Neurosci* 30:14972-14979.
- 1260 Ross G (2004) The public health implications of polychlorinated biphenyls (PCBs) in the environment.
1261 *Ecotoxicol Environ Saf* 59:275-291.
- 1262 Roveda AM, Veronesi L, Zoni R, Colucci ME, Sansebastiano G (2006) [Exposure to polychlorinated
1263 biphenyls (PCBs) in food and cancer risk: recent advances]. *Ig Sanita Pubbl* 62:677-696.
- 1264 Sadowski RN, Stebbings KA, Slater BJ, Bandara SB, Llano DA, Schantz SL (2016) Developmental exposure
1265 to PCBs alters the activation of the auditory cortex in response to GABA. *Neurotoxicology* 56:86-
1266 93.
- 1267 Safe S (1993) Toxicology, structure-function relationship, and human and environmental health impacts
1268 of polychlorinated biphenyls: progress and problems. *Environ Health Perspect* 100:259-268.
- 1269 Saldaña E, Feliciano M, Mugnaini E (1996) Distribution of descending projections from primary auditory
1270 neocortex to inferior colliculus mimics the topography of intracollicular projections. *J Comp*
1271 *Neurol* 371:15-40.
- 1272 Samson J, Wiktorek-Smagur A, Politsanski P, Rajkowska E, Pawlaczyk-Luszczynska M, Dudarewicz A, Sha
1273 SH, Schacht J, Sliwinska-Kowalska M (2008) Noise-induced time-dependent changes in oxidative
1274 stress in the mouse cochlea and attenuation by D-methionine. *Neuroscience* 152:146-150.
- 1275 Schofield BR, Beebe NL (2019) Subtypes of GABAergic cells in the inferior colliculus. *Hear Res* 376:1-10.
- 1276 Scholl B, Wehr M (2008) Disruption of balanced cortical excitation and inhibition by acoustic trauma. *J*
1277 *Neurophysiol* 100:646-656.
- 1278 Schreiner CE, Winer JA (2005) *The inferior colliculus*: Springer Science+ Business Media, Incorporated.
- 1279 Selvakumar K, Bavithra S, Krishnamoorthy G, Venkataraman P, Arunakaran J (2012) Polychlorinated
1280 biphenyls-induced oxidative stress on rat hippocampus: a neuroprotective role of quercetin.
1281 *ScientificWorldJournal* 2012:980314.
- 1282 Sokoloff L (1981) Localization of functional activity in the central nervous system by measurement of
1283 glucose utilization with radioactive deoxyglucose. *J Cereb Blood Flow Metab* 1:7-36.
- 1284 Song L, McGee J, Walsh EJ (2008) The influence of thyroid hormone deficiency on the development of
1285 cochlear nonlinearities. *J Assoc Res Otolaryngol* 9:464-476.
- 1286 Spreng M (2000) Central nervous system activation by noise. *Noise Health* 2:49-58.
- 1287 Stiebler I, Neulist R, Fichtel I, Ehret G (1997) The auditory cortex of the house mouse: left-right
1288 differences, tonotopic organization and quantitative analysis of frequency representation. *J*
1289 *Comp Physiol A* 181:559-571.
- 1290 Sturm JJ, Zhang-Hooks YX, Roos H, Nguyen T, Kandler K (2017) Noise Trauma-Induced Behavioral Gap
1291 Detection Deficits Correlate with Reorganization of Excitatory and Inhibitory Local Circuits in the
1292 Inferior Colliculus and Are Prevented by Acoustic Enrichment. *J Neurosci* 37:6314-6330.
- 1293 Sullivan JR, Delfino JJ, Buelow CR, Sheffy TB (1983) Polychlorinated biphenyls in the fish and sediment of
1294 the Lower Fox River, Wisconsin. *Bull Environ Contam Toxicol* 30:58-64.
- 1295 Syka J, Popelár J, Kvasnák E, Astl J (2000) Response properties of neurons in the central nucleus and
1296 external and dorsal cortices of the inferior colliculus in guinea pig. *Exp Brain Res* 133:254-266.
- 1297 Szczepaniak WS, Møller AR (1996) Evidence of neuronal plasticity within the inferior colliculus after
1298 noise exposure: a study of evoked potentials in the rat. *Electroencephalogr Clin Neurophysiol*
1299 100:158-164.
- 1300 Sziklai I (2004) The significance of the calcium signal in the outer hair cells and its possible role in tinnitus
1301 of cochlear origin. *Eur Arch Otorhinolaryngol* 261:517-525.

- 1302 Tabuchi K, Nakamagoe M, Nishimura B, Hayashi K, Nakayama M, Hara A (2011) Protective effects of
1303 corticosteroids and neurosteroids on cochlear injury. *Med Chem* 7:140-144.
- 1304 Tamamaki N, Yanagawa Y, Tomioka R, Miyazaki J, Obata K, Kaneko T (2003) Green fluorescent protein
1305 expression and colocalization with calretinin, parvalbumin, and somatostatin in the GAD67-GFP
1306 knock-in mouse. *J Comp Neurol* 467:60-79.
- 1307 Tatone C, Carbone MC, Falone S, Aimola P, Giardinelli A, Caserta D, Marci R, Pandolfi A, Ragnelli AM,
1308 Amicarelli F (2006) Age-dependent changes in the expression of superoxide dismutases and
1309 catalase are associated with ultrastructural modifications in human granulosa cells. *Mol Hum
1310 Reprod* 12:655-660.
- 1311 Turner J, Larsen D, Hughes L, Moechars D, Shore S (2012) Time course of tinnitus development following
1312 noise exposure in mice. *J Neurosci Res* 90:1480-1488.
- 1313 Uziel A (1986) Periods of sensitivity to thyroid hormone during the development of the organ of Corti.
1314 *Acta Otolaryngol Suppl* 429:23-27.
- 1315 Vaithiyalingam Chandra Sekaran N, Deshpande MS, Ibrahim BA, Xiao G, Shinagawa Y, Llano DA (2021)
1316 Patterns of Unilateral and Bilateral Projections From Layers 5 and 6 of the Auditory Cortex to the
1317 Inferior Colliculus in Mouse. *Front Syst Neurosci* 15:674098.
- 1318 Vega-López A, Galar-Martínez M, Jiménez-Orozco FA, García-Latorre E, Domínguez-López ML (2007)
1319 Gender related differences in the oxidative stress response to PCB exposure in an endangered
1320 goodeid fish (*Girardinichthys viviparus*). *Comp Biochem Physiol A Mol Integr Physiol* 146:672-
1321 678.
- 1322 Vogler DP, Robertson D, Mulders WH (2014) Hyperactivity following unilateral hearing loss in
1323 characterized cells in the inferior colliculus. *Neuroscience* 265:28-36.
- 1324 Wang H, Brozoski TJ, Caspary DM (2011) Inhibitory neurotransmission in animal models of tinnitus:
1325 maladaptive plasticity. *Hear Res* 279:111-117.
- 1326 Wang J, Salvi RJ, Powers N (1996) Plasticity of response properties of inferior colliculus neurons
1327 following acute cochlear damage. *J Neurophysiol* 75:171-183.
- 1328 Weber R, Herold C, Hollert H, Kamphues J, Ungemach L, Blepp M, Ballschmiter K (2018) Life cycle of
1329 PCBs and contamination of the environment and of food products from animal origin. *Environ
1330 Sci Pollut Res Int* 25:16325-16343.
- 1331 Wei S (2013) Peripheral Hearing Loss Causes Hyperexcitability of the Inferior Colliculus. *Journal of
1332 Otology* 8:39-43.
- 1333 Weintraub M, Birnbaum LS (2008) Catfish consumption as a contributor to elevated PCB levels in a non-
1334 Hispanic black subpopulation. *Environ Res* 107:412-417.
- 1335 Wharton JA, Church GT (1990) Influence of menopause on the auditory brainstem response. *Audiology*
1336 29:196-201.
- 1337 Willard FH, DK R (1983) Anatomy of the central auditory system. In: *The auditory psychobiology of the
1338 mouse*. (JF W, ed), pp 201-304. Springfield, IL: Thomas.
- 1339 Winer JA, Larue DT, Diehl JJ, Hefti BJ (1998) Auditory cortical projections to the cat inferior colliculus. *J
1340 Comp Neurol* 400:147-174.
- 1341 Wong AB, Borst JGG (2019) Tonotopic and non-auditory organization of the mouse dorsal inferior
1342 colliculus revealed by two-photon imaging. *Elife* 8.
- 1343 Wong PW, Brackney WR, Pessah IN (1997) Ortho-substituted polychlorinated biphenyls alter microsomal
1344 calcium transport by direct interaction with ryanodine receptors of mammalian brain. *J Biol
1345 Chem* 272:15145-15153.
- 1346 Wu YC, Hsieh RP, Lü YC (1984) Altered distribution of lymphocyte subpopulations and augmentation of
1347 lymphocyte proliferation in chronic PCB poisoned patients. *Zhonghua Min Guo Wei Sheng Wu Ji
1348 Mian Yi Xue Za Zhi* 17:177-187.

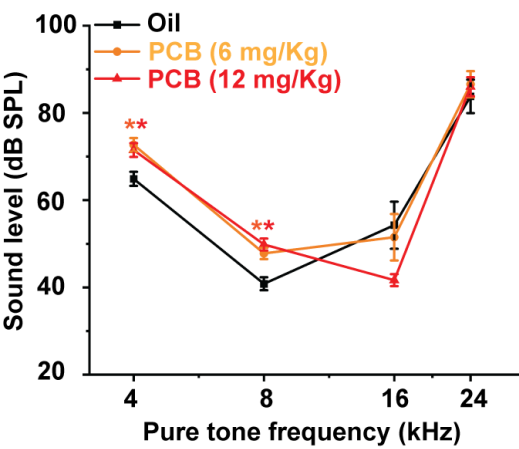
- 1349 Xie XL, Zhou WT, Zhang KK, Yuan Y, Qiu EM, Shen YW, Wang Q (2019) PCB52 induces hepatotoxicity in
1350 male offspring through aggravating loss of clearance capacity and activating the apoptosis: Sex-
1351 biased effects on rats. *Chemosphere* 227:389-400.
- 1352 Yuditsev G, Asilador AR, Sons S, Vaithiyalingam Chandra Sekaran N, Coppinger M, Nair K, Prasad M,
1353 Xiao G, Ibrahim BA, Shinagawa Y, Llano DA (2021) Evidence for Layer-Specific Connectional
1354 Heterogeneity in the Mouse Auditory Corticocollicular System. *J Neurosci* 41:9906-9918.
- 1355 Zeller K, Rahner-Welsch S, Kuschinsky W (1997) Distribution of Glut1 glucose transporters in different
1356 brain structures compared to glucose utilization and capillary density of adult rat brains. *J Cereb*
1357 *Blood Flow Metab* 17:204-209.
- 1358 Zeng L, Yang Y, Hu Y, Sun Y, Du Z, Xie Z, Zhou T, Kong W (2014) Age-related decrease in the
1359 mitochondrial sirtuin deacetylase Sirt3 expression associated with ROS accumulation in the
1360 auditory cortex of the mimetic aging rat model. *PLoS One* 9:e88019.
- 1361 Zhao Y, Song Q, Li X, Li C (2016) Neural Hyperactivity of the Central Auditory System in Response to
1362 Peripheral Damage. *Neural Plast* 2016:2162105.
- 1363 Zheng QY, Johnson KR, Erway LC (1999) Assessment of hearing in 80 inbred strains of mice by ABR
1364 threshold analyses. *Hear Res* 130:94-107.
- 1365

A

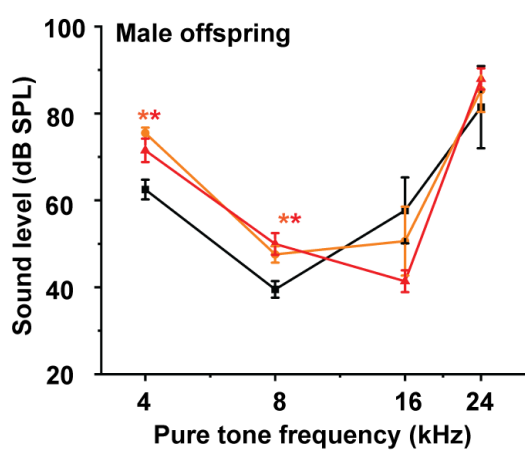
Experimental design



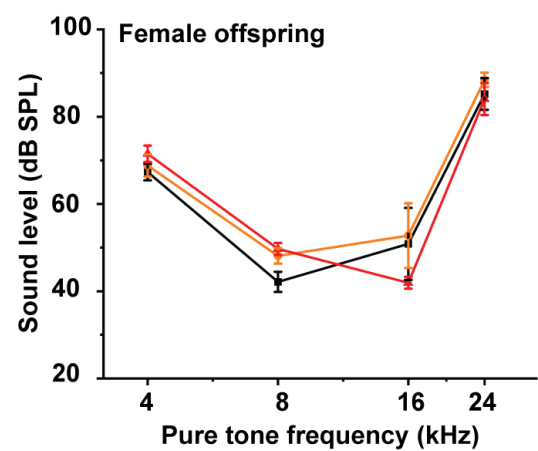
B



C

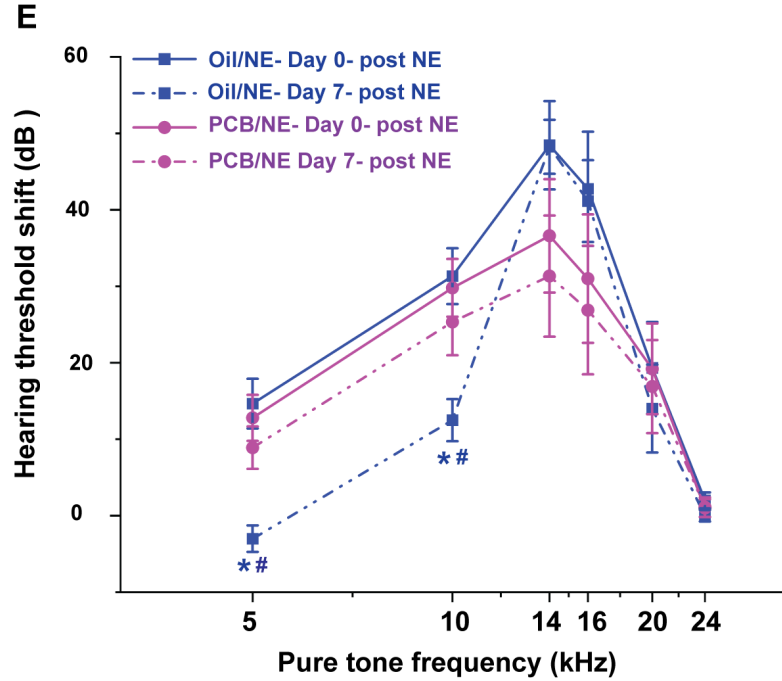
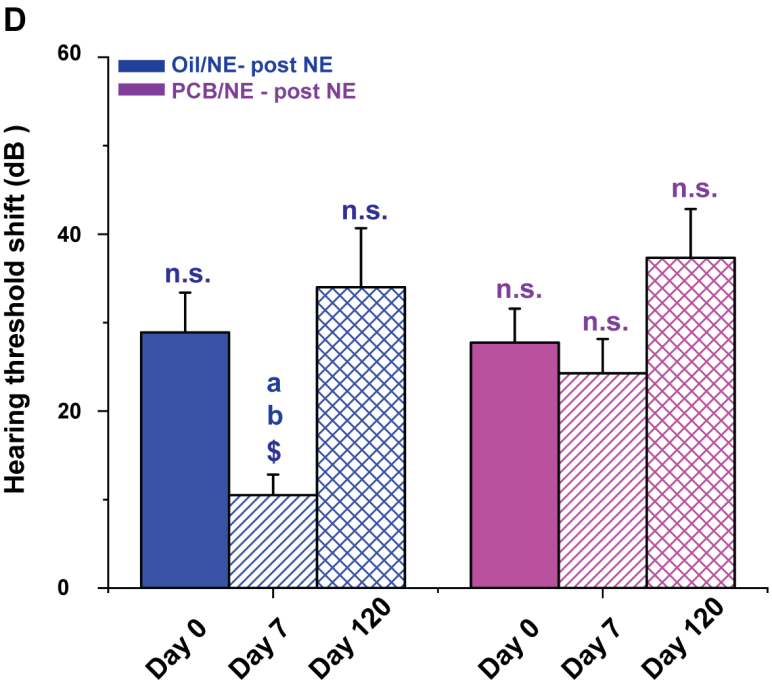
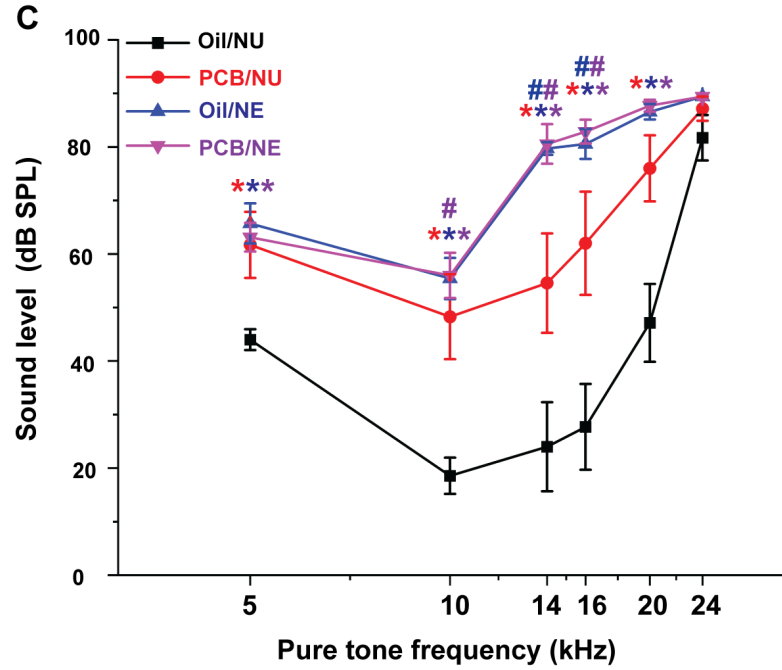
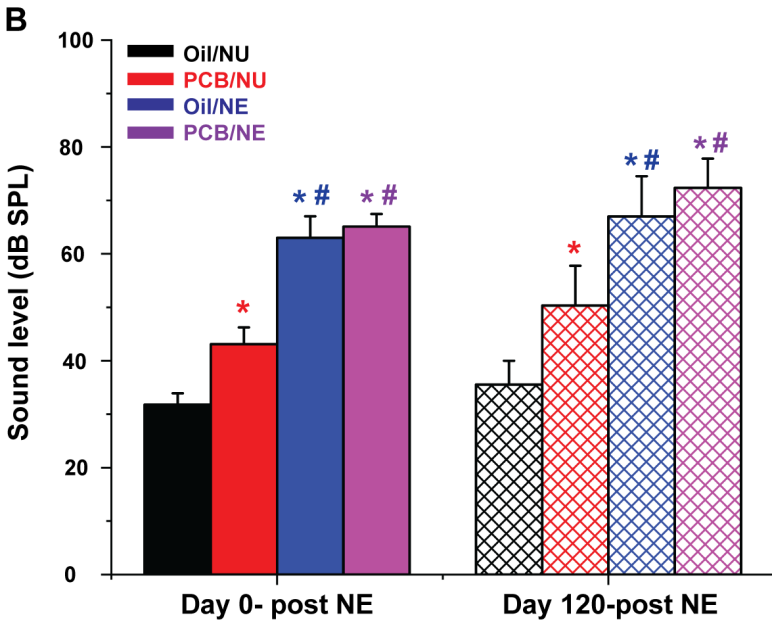
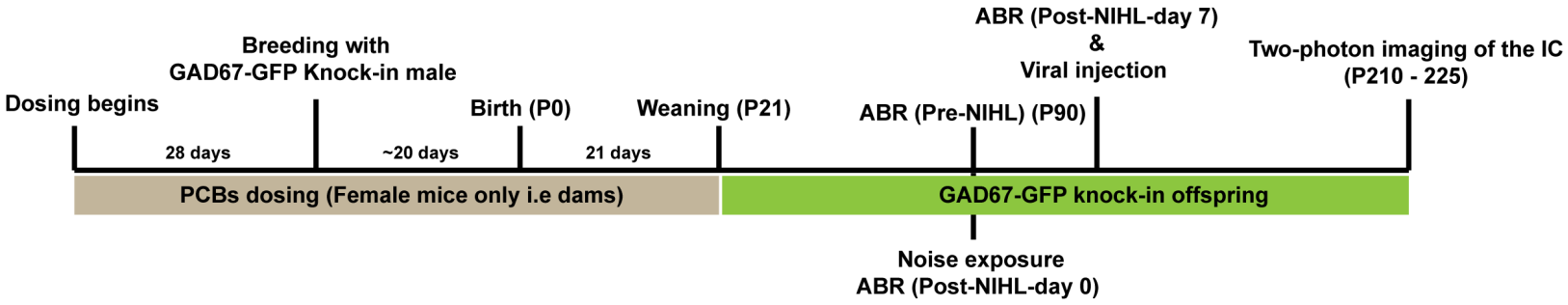


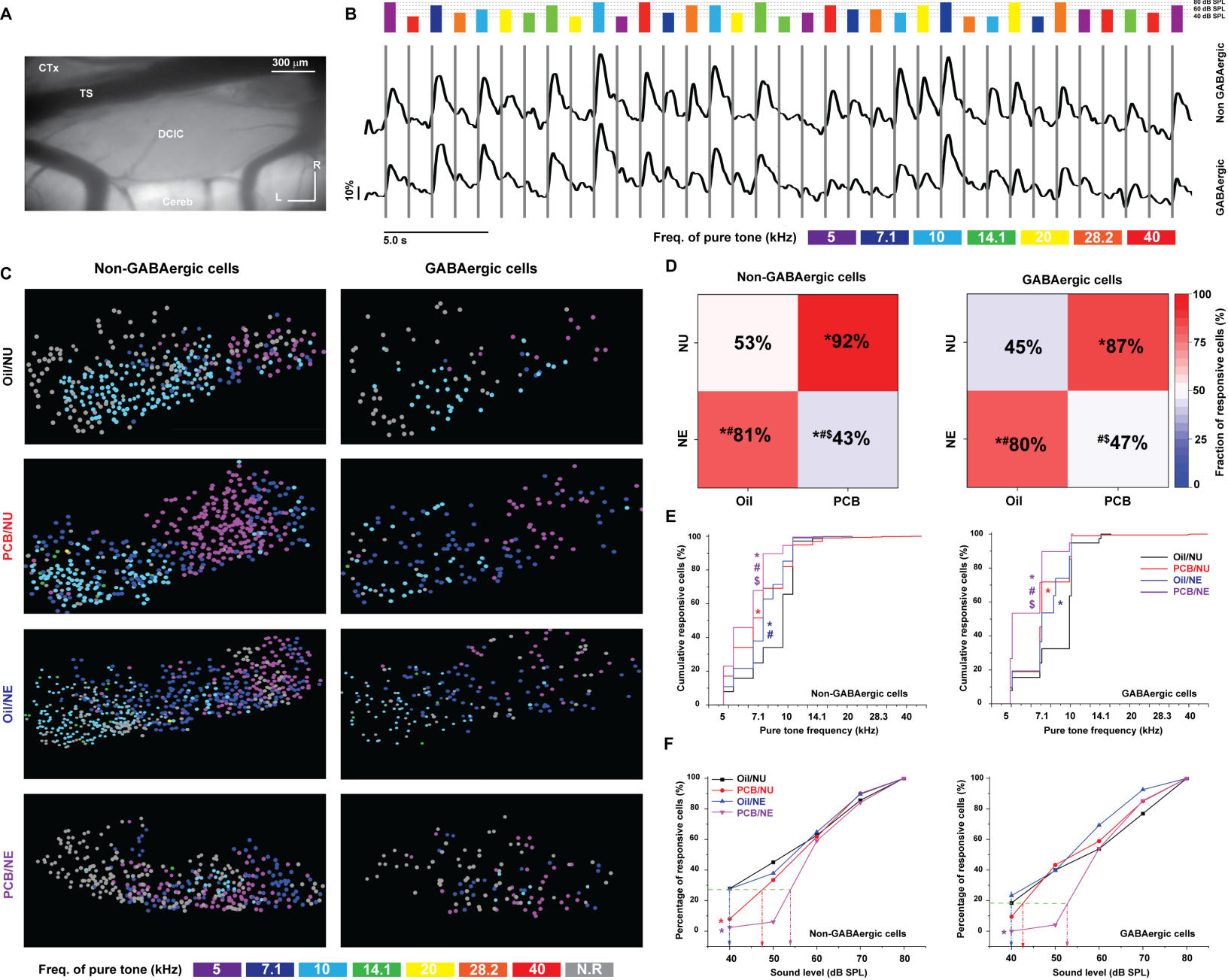
D



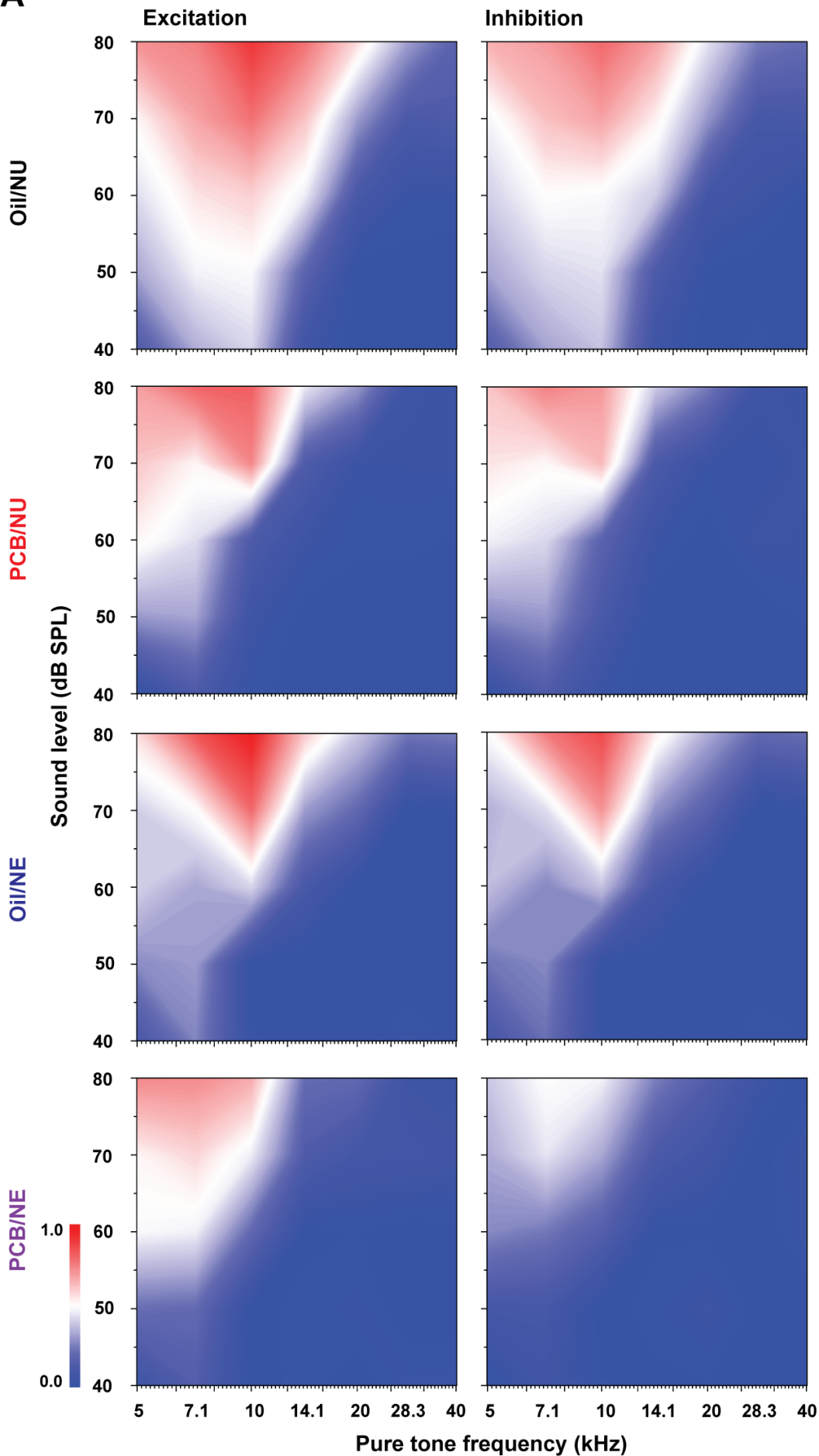
A

Experimental design

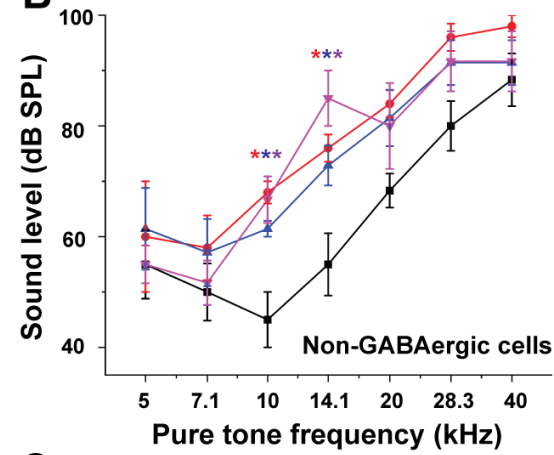




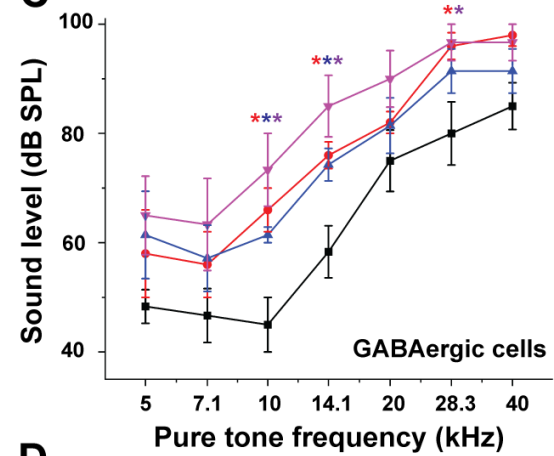
A



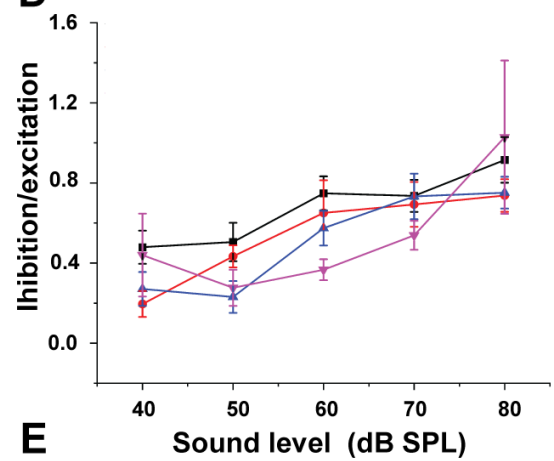
B



C



D



E

